

# Formation of ultra-compact dwarf galaxies: tests of the galaxy threshing scenario in Fornax

P. A. Thomas<sup>1\*</sup>, M. J. Drinkwater<sup>2</sup> and E. Evstigneeva<sup>2</sup>

<sup>1</sup>*Astronomy Centre, University of Sussex, Falmer, Brighton BN1 9QH*

<sup>2</sup>*Department of Physics, University of Queensland, QLD 4072, Australia*

29 October 2018

## ABSTRACT

This paper investigates the possibility that UCD galaxies in the Fornax cluster are formed by the threshing of nucleated, early-type dwarf galaxies (hereafter dwarf galaxies).

Similar to the results of Côté et al. (2006) for the Virgo cluster, we show that the Fornax Cluster observations are consistent with a single population in which all dwarfs are nucleated, with a ratio of nuclear to total magnitude that varies slowly with magnitude. Importantly, the magnitude distribution of the UCD population is similar to that of the dwarf nuclei in the Fornax cluster.

The joint population of UCDs and the dwarfs from which they may originate is modelled and shown to be consistent with an NFW profile with a characteristic radius of 5 kpc. Furthermore, a steady-state dynamical model reproduces the known mass profile of Fornax. However, there are a number of peculiarities in the velocity dispersion data that remain unexplained.

The simplest possible threshing model is tested, in which dwarf galaxies move on orbits in a static cluster potential and are threshed if they pass within a radius at which the tidal force from the cluster exceeds the internal gravity at the core of their dark matter halo. This fails to reproduce the observed fraction of UCDs at radii greater than 30 kpc from the core of Fornax.

**Key words:** galaxies: dwarf – galaxies: formation – methods: analytical

## 1 INTRODUCTION

In recent years considerable evidence has accumulated that disruptive processes play an important role in galaxy evolution as well as the more dominant hierarchical merging. Observational evidence for these disruptive processes is particularly evident in the dense environment of galaxy clusters. The evidence includes populations of individual intra-cluster objects such as planetary nebulae (Arnaboldi et al. 2004; Feldmeier et al. 2004a) and red giant stars (Durrell et al. 2002), as well as the general diffuse light now thought to make up a significant fraction of the total stellar mass in clusters (Feldmeier et al. 2004a; Feldmeier et al. 2004b; Gonzalez, Zabludoff, & Zaritsky 2005; Zibetti et al. 2005).

In this paper we focus on a relatively new component of intra-cluster space, ultra-compact dwarf (UCD) galaxies. These are compact systems of old stars akin to globular clusters but they are 10–100 times more luminous than Galactic globular clusters and they are located in intra-cluster

space between galaxies. The first UCDs were discovered in the Fornax Cluster independently in studies of globular clusters (Minniti et al. 1998; Hilker, Infante, & Vieira 1999) and in studies of compact dwarf galaxies (Drinkwater et al. 2000b; Phillipps et al. 2001). The UCDs are unlike any known galaxies in terms of luminosity, morphology and size (Drinkwater et al. 2003). Several hypotheses have been suggested to explain the origin of UCDs ranging from them being the high-luminosity end of a putative intra-cluster globular cluster distribution, to being the evolved super star clusters formed in galaxy merger events. In this paper we focus on the model that UCDs are formed by the global tidal field of a cluster which can strip, or “thresh”, the outer stellar envelopes of nucleated dwarf galaxies (dE,Ns and dS0,Ns) as they pass repeatedly through the inner regions of a cluster leaving just the bare nucleus to survive as a UCD (Bekki, Couch, & Drinkwater 2001; Bekki et al. 2003; Goerdt et al. 2007)

The motivation for the current work is the subsequent discovery of a larger population of fainter UCDs in the central region of the Fornax Cluster (Drinkwater et al. 2004;

\* Email: p.a.thomas@sussex.ac.uk

Gregg et al. 2008). This sample of 60 UCDs is large enough to permit us to test several aspects of the threshing hypothesis using a statistically significant sample. Our focus will be to test simple aspects of the distributions of the UCD and galaxy populations. An alternative approach based on the internal properties of the UCDs is also in progress (e.g. Evstigneeva et al. 2007).

Our basic premise for this paper is that if UCDs are descendants of disrupted galaxies, then the UCD parent population can be modelled by the combined *current* population of Fornax cluster UCDs and dwarf galaxies. We test whether the observed spatial and velocity distributions of the two populations are consistent with this hypothesis and conclude that they are. We then model the orbits of UCDs/galaxies drawn from this joint population to determine what fraction of them pass close enough to the cluster centre to lead to threshing. The relative fraction UCDs to dwarfs seen at large radii in Fornax is inconsistent with this static threshing model.

In Section 2 we define the UCD and galaxy samples for our analysis. In Section 3 we test if the luminosity function of the UCDs is consistent with them having been drawn as random sample from the nuclei of dwarf galaxies in the cluster. Section 4 develops a dynamical model for the joint population, and Section 5 calculates the fraction of threshed orbits at each radius. Finally, in Section 6, we summarise our results and draw conclusions about the plausibility of the threshing hypothesis.

We adopt a distance of 20 Mpc to the Fornax Cluster (Drinkwater, Gregg, & Colless 2001a) corresponding to a distance modulus of 31.51 magnitudes. In this paper we are not concerned with late-type galaxies. To avoid endless repetition, we use the terms galaxy and dwarf to refer to early-type objects only, as defined in Section 2.1.

## 2 DATA SAMPLES FROM THE FORNAX CLUSTER

### 2.1 Early-type galaxy sample

The hypothesis that we test in this paper is that UCDs form from the disruption of nucleated dwarf galaxies. Our authority for the morphological classification of Fornax Cluster galaxies is the *Fornax Cluster Catalog* (FCC, Ferguson 1989) which was based on photographic data. The FCC lists some 291 galaxies as early types (i.e. not Sa-d, Sm or Im; we include spheroidal galaxies in our sample). Of these, 103 are classified as nucleated. Recent *Hubble Space Telescope* imaging results from the ACS Virgo Cluster Survey (Côté et al. 2006, hereafter CPF06) suggest that the frequency of nucleation in early type galaxies is actually much higher than suggested from the photographic ground-based surveys. Faint nuclei are difficult to detect because they are washed out by atmospheric seeing and the central regions of the brightest galaxies are saturated. Notably, CPF06 suggest that potentially *all* dwarf galaxies may contain nuclei. We apply the CPF6 model to our Fornax data in Section 3.1 and show that the observed fraction of nucleated dwarfs as a function of magnitude is consistent with this assumption. Also, the spatial distributions of nucleated and non-nucleated dwarfs, shown in Fig. 4, are indistinguishable.

For the purposes of this current work, therefore, we define the parent galaxy sample to be all early-type dwarf galaxies listed as definite or probable members in the FCC. Where radial velocities are known, we use these to define membership, otherwise we use the FCC membership classifications. New radial velocities result in the removal of some FCC-classified members and the inclusion of some FCC-classified background galaxies now known to be members (e.g. see Drinkwater et al. 2001b). More recent radial velocity measurements are taken from Karick, Drinkwater, & Gregg (2003). Where the classification is uncertain, we have taken all galaxies fainter than  $M_B = -14$  as dwarf; the maximum magnitude for a normal galaxy is then  $M_B = -16.3$  and the minimum magnitude for a dwarf galaxy is  $M_B = -17.8$ . A complete list of the galaxies is given in Table A1.

The galaxies in our sample have morphological classifications from the FCC which can include a flag that they are nucleated. We use these flags in our discussion below, but we emphasise that there is no HST imaging for most of these galaxies, so we cannot tell with certainty if a given galaxy is really nucleated. We instead adopt the general result of CPF06 that all dwarf galaxies have nuclei, with a magnitude that is related to that of the host galaxy (see Section 3.1 below).

The dwarf galaxy sample that we use is effectively complete to a limit of around  $M_B = -13.5$  (see FCC). The velocity data used to confirm cluster membership are complete for galaxies brighter than  $M_B = -16$  and become 50 per cent complete at  $M_B = -14.5$ .

### 2.2 UCD sample

The UCDs were originally discovered as part of the all-object Fornax Cluster Spectroscopic Survey (Drinkwater et al. 2000a). Although the original survey measured all objects (to  $b_J < 19.8$ ), this was subsequently extended in a selective search at fainter limits specifically designed to find UCDs. The selected search used a slightly smaller field: a radius limit of 0.9 degrees (314 kpc) around the central cluster galaxy NGC 1399. The selected search also used a restricted colour range of  $b_J - r_F < 1.7$  for objects with both  $b_J$  and  $r_F$  values measured; for fainter objects with no  $r_F$  values, no colour criterion was applied. This colour selection served to remove Galactic M-dwarf stars from the sample: no UCDs have colours in this range. The completeness of the spectroscopic observations is given as a function of magnitude in Table 1.

The  $b_J$  photographic APM magnitudes were converted to  $m_B$  magnitudes by the approximate relation  $m_B = b_J + 0.20$  (based on the Blair & Gilmore 1982 relation of  $b_J = B - 0.28(B - V)$  for an average dwarf galaxy colour of  $B - V = 0.7$ ) so that  $M_B = b_J + 0.20 - 31.51 = b_J - 31.31$ .

The spatial locations of the UCDs are far from circularly symmetric about the centre of Fornax but tend to lie in a band running from North East to South West (see fig. 2 in Gregg et al. 2008). This presumably reflects the infall pattern onto the cluster. Provided that the distribution is relaxed then this will not affect the dynamical modelling; however it may confuse the relation between the true three-dimensional positions and velocities and the observed ones.

**Table 1.** Spectroscopic completeness of the UCD sample. Completeness,  $C$ , is defined as the fraction of UCD targets for which redshifts were measured.  $N_{\text{UCD}}$ , in two bins of projected radius  $r$ , is the number of UCDs found in each magnitude range. The actual number of UCDs can therefore be estimated as  $N_{\text{UCD}}/C$ .

$b_J$ range	$M_B$ range	$C$	$N_{\text{UCD}}$	
			$r < 17.5$ kpc	$r > 17.5$ kpc
16.0–20.5	–15.3 to –10.8	0.94	0	21
20.5–21.0	–10.8 to –10.3	0.81	6	14
21.0–21.5	–10.3 to –9.8	0.35	5	14

For the purposes of modelling in this paper, we assume a spherically-symmetric distribution.

### 2.3 Joint sample selection

According to our central hypothesis, there was an original parent population of dwarf galaxies, some of which were subsequently disrupted to form UCDs. Unfortunately the selection effects are different for the two sub-populations and so we need to use different samples for different parts of our analysis. This will be described at the beginning of each relevant section. Here we make a few general comments on the relative spatial extent of the dwarf and UCD samples.

The FCC is a wide-field survey. It covers a rectangular region with a largest inscribed circle that extends to a radius of 3 degrees (1.05 Mpc) from the cluster centre. Our main UCD sample is limited to a smaller region defined by a maximum radius of 0.9 degrees (314 kpc) from the cluster centre. We have modelled the density distribution and estimate that there may be up to 6 missing UCDs at larger radii (although, for the brighter UCDs, two additional regions extending to a radius of 3 degrees have been surveyed and no UCDs were found). Adding 6 extra UCDs with the appropriate density distribution makes very little difference to the modelling of the spatial distribution of the joint UCD plus dwarf population in Section 4.1 below.

For the UCDs there is also a need to exclude those at very small radii from the central cluster galaxy, NGC 1399. The distribution of UCD radial velocities shown in Fig. 1 shows a trend to smaller velocities (and velocity dispersion) at low radius. The inner UCDs are clearly moving in the galactic and not the cluster potential and could be considered as bright globular clusters attached to NGC1399. The choice of where to draw the dividing line between galactic and intracluster UCDs is somewhat arbitrary. We cut at 3 arcmin (17.5 kpc) which excludes 11 UCDs from our sample (see Table 1), including the two relatively low-velocity UCDs seen in the figure at a radius and velocity of approximately 15 kpc and  $1140 \text{ km s}^{-1}$ , respectively. (Including these two in our analysis makes little difference to the results and would leave the velocity dispersion of the excluded clusters as formally zero once the velocity errors have been accounted for.)

For reasons that we shall describe later in Section 3.2, we divide the dwarf population into two. “Bright dwarfs” with  $M_B < -15.0$  are those that correspond to the progenitors of UCDs in our model, whereas “faint dwarfs” would give UCDs that fall below our magnitude limit. Table 2 gives the number of galaxies of each type in different radial bins.

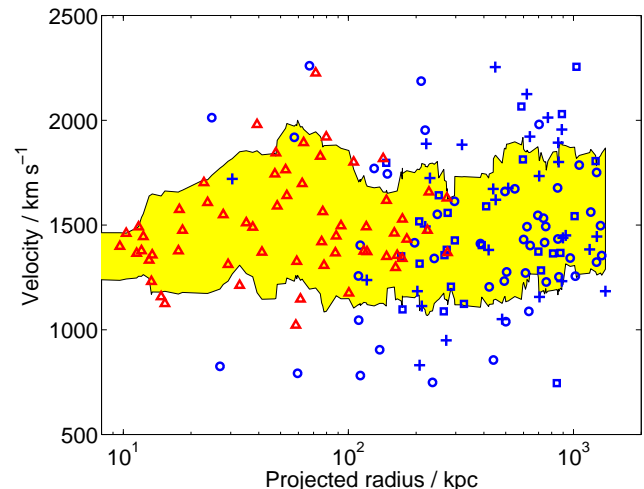


**Figure 1.** A comparison of the UCD and galaxy populations. The radial velocities are plotted as a function of projected radius. UCDs are shown as red triangles, normal galaxies as blue squares, and dwarfs brighter and fainter than  $M_B = -15.0$  as blue circles and crosses, respectively. The yellow shaded area shows a running mean of the 1-sigma velocity dispersion.

**Table 2.** Number of Fornax galaxies of different types in different annular bins centred on NGC1399. The division between bright and faint dwarfs is taken as  $M_B = -15.0$ .

Sample	Radial range in kpc		
	17.5–314	314–1050	1050–1500
UCDs	49	0	0
Normal galaxies	13	13	4
Bright dwarfs	11	22	5
Faint dwarfs	65	129	28

## 3 COMPARISON OF LUMINOSITY DISTRIBUTIONS

In this section we develop a unified model for nucleated and non-nucleated dwarf galaxies whereby all galaxies have nuclei but only a fraction of these are bright enough to be detected and classified as such in the FCC. We then go on to compare the predicted luminosity function of nuclei with that of UCDs. As we are interested only in the shape of the magnitude distributions, we use the full samples of dwarfs and UCDs even though two extend over different spatial regions.

### 3.1 Early-type nuclei

An important property of the parent galaxies is the luminosity distribution of the galaxy nuclei as these will be compared to the UCD luminosities. We cannot directly measure the luminosities of galaxy nuclei in the Fornax Cluster because most do not have high-resolution HST imaging. Instead we take a statistical approach: we assume that *all* dwarf galaxies host nuclei and infer the nuclear luminosities from the total galaxy luminosities.

CPF06 measured nuclear luminosities for 51 dwarf galaxies in the Virgo Cluster. They confirmed previous sug-

gestions that the nuclear luminosities increase with the galaxy luminosity. They modelled this relation as both a fixed offset between the nuclear and total magnitudes,  $g'_{\text{nuc}} = g'_{\text{gal}} + (6.25 \pm 0.21)$ , and an offset slowly varying with magnitude,  $g'_{\text{nuc}} = (0.90 \pm 0.18)g'_{\text{gal}} + (7.59 \pm 2.50)$ . We note that our galaxy sample extends to much fainter magnitudes than did the Virgo sample studied by CPF06, and so we will have to extrapolate their relation. We therefore allow the slope of the relation to vary, but require that it go through the mid point of the CPF06 data ( $g'_{\text{gal}}, g'_{\text{nuc}} = 13.40, 19.65$ ) defined by the crossing point of their two relations.

We model the scatter in the relationship by adding a random normal variable with a mean of zero and a standard deviation of 1.5 to the derived nuclear magnitude. The standard deviation was inferred from the scatter about the fixed-slope fit of CPF06 (their equation 15).

To convert the ACS  $g'$  photometry to absolute magnitudes we first use the mean value of  $B_T - g = 0.30$  for the ACS dwarf galaxies to convert  $g$  magnitudes to  $B_T$ . We then apply the distance modulus of 31.09 magnitudes quoted by CPF06, obtaining  $M_B = g' - 30.79$ .

To constrain the slope of the  $g'_{\text{nuc}} - g'_{\text{gal}}$  relation, we require that it predicts the correct distribution of galaxies that we would expect to have been classified as nucleated in the photographic FCC survey. For each galaxy, we predict its nuclear luminosity as above, then we classify it as nucleated if the nucleus is brighter than the point-source detection limit on the photographic plate (approximately  $B_T = 22.6$  or  $M_B = -8.9$  for the FCC; H. Ferguson, private communication).

The results, shown in Fig. 2, show that this model can nicely predict the luminosity distribution of the early-type galaxies that are classified as nucleated in the photographic FCC survey. To produce the figure, we used a slope of 0.7, smaller than the best fit of CPF06.<sup>1</sup> The nuclear-to-total magnitude relation becomes

$$M_{B_{\text{nuc}}} + 11.14 = 0.7(M_{B_{\text{gal}}} + 17.39). \quad (1)$$

The leftmost, blue bars in the figure show the magnitude distribution of all dwarfs. We averaged over 100 realisations of the scatter in the relation to obtain the prediction for observable, nucleated dwarfs shown in the green, middle bars of the figure. These are statistically indistinguishable from the actual number of dwarfs classified as nucleated, shown in the rightmost, brown bars.

We show in Section 4.1 below that the spatial distributions of the nucleated and non-nucleated dwarfs are identical, thus lending further support to the hypothesis that the presence of a detectable nucleus is the only difference between them.

<sup>1</sup> It is not clear as to whether the CPF06 data will accept a slope of 0.7: we can also get an acceptable fit if we use a slope of 0.9 for the relation, provided that the magnitude limit for point-source detection is raised to  $-8.5$ .

If we extend our analysis to include normal galaxies then we predict far more nucleated galaxies than are observed. This seems to be in disagreement with the results from Virgo; however it is possible that brightest nuclei would be saturated on the photographic plate and so hard to detect: we note that CPF06 find many more nuclei in bright galaxies with  $M_B \leq -17.4$ , than did photographic surveys.

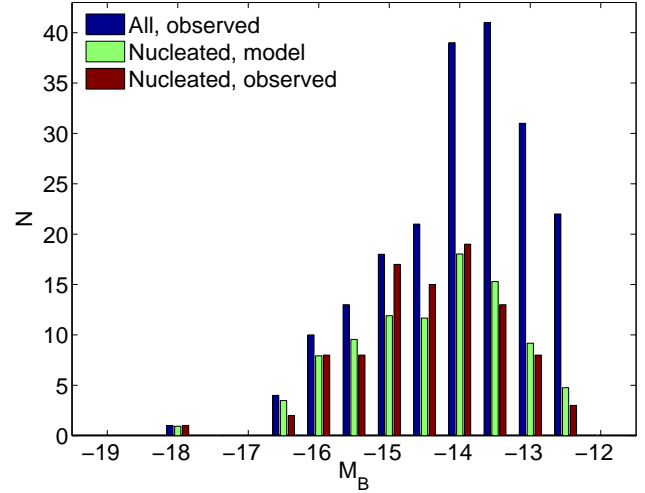


**Figure 2.** The distribution of dwarf galaxies classified as “nucleated”. The leftmost, blue bars show the observed magnitudes of all Fornax dwarfs. The middle, green bars show only those whose predicted nuclear magnitudes would be greater than  $-8.9$  according to the model developed in the text. Finally, the rightmost, brown bars show the actual magnitude distribution of nucleated dwarfs in Fornax.

### 3.2 UCDs

From the observed dwarf population, we can now predict the distribution of nuclear magnitudes. If we assume that the threshing process is independent of galactic (and nuclear) luminosity, then these should have the same *shape* of distribution as the UCDs. Furthermore, the relative normalisation should tell us what fraction of the dwarfs have been threshed. The predicted and actual UCD distributions are given in Fig 3. Note that the predicted numbers from our model have been scaled down by the completeness values in Table 1 to allow for the fraction of unmeasured objects.

The figure shows that the predicted luminosity distribution of UCDs is not perfect. The model seems to give an excess of UCDs brighter than  $M_B = -11.25$  as compared to fainter ones. It is hard to assess the significance of this: given the relatively small number of objects and the uncertainties in the relationship between galactic and nuclear magnitudes, it is probably acceptable.

The model predicts that 38 dwarfs should have nuclei that correspond to observable UCDs. This motivates our selection of  $M_B = -15.0$  as the dividing line between bright and faint dwarfs, as this gives 38 bright dwarfs. Without scatter, equation 1 would have predicted a brighter limit,  $M_B \approx -15.8$ , but the greater number of faint galaxies biases things towards fainter magnitudes. Of these 38 dwarfs, only 11 lie within 314 kpc. Thus the model predicts that the vast majority of dwarfs within this region are likely to be threshed. Even when averaged over the whole sample, more than half the dwarf population should be threshed.

## 4 A DYNAMICAL MODEL FOR THE JOINT DWARF/UCD POPULATION

This section constructs a model of the three-dimensional density distribution of the joint dwarf/UCD population in

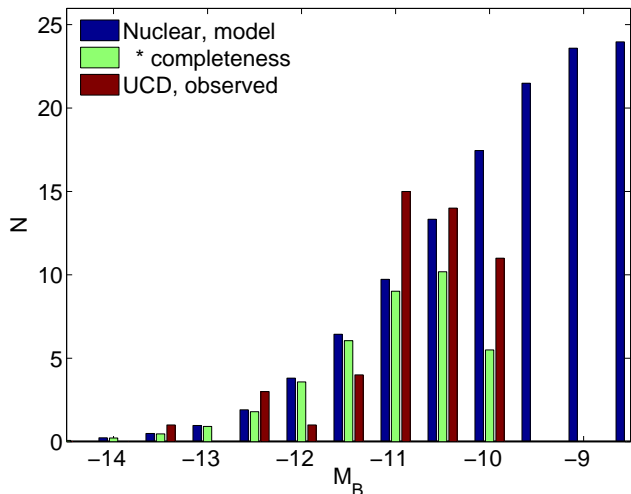


**Figure 3.** The leftmost, blue bars show the predicted distribution of nuclear magnitudes for Fornax dwarfs, averaged over 100 realisations: the middle, green bars multiply this by the completeness factor for UCD observations. If the threshing hypothesis is correct then this should be proportional to the rightmost, brown bars that show the observed distribution of UCD magnitudes.

the cluster. There will turn out to be some degeneracy in the models which we will attempt to constrain by matching them to observed mass models for Fornax.

When comparing dwarfs and UCDs, we restrict our attention to the bright dwarfs,  $M_B < -15.0$ , as described in the previous section. We will show that the joint UCD + bright dwarf population is well-fit by an NFW model (Navarro, Frenk & White 1997) in dynamical equilibrium in the cluster potential.

#### 4.1 Spatial distributions

We first compare the spatial distribution of nucleated and non-nucleated dwarfs. If we plot all the dwarf galaxies together, as in Fig. 4, the nucleated dwarfs are shown to be very slightly more centrally concentrated. This is in the same sense as was originally reported for the dwarf galaxies of the Virgo (Binggeli, Tammann, & Sandage 1987) and Fornax (Ferguson & Sandage 1989) Clusters, but for our present sample the difference is not significant (the Kolmogorov–Smirnov test returns a probability that the two are drawn from the same distribution of 0.2). As expected from our discussion above, the nucleated dwarfs are significantly more luminous on average than the non-nucleated dwarfs: the difference in radial distributions is actually a luminosity bias. If, instead, we compare the distributions of dwarfs of the same luminosity ( $M_B > -15$ ), then the difference is removed entirely. This observation strengthens the hypothesis of the previous section, that dwarfs classified as nucleated or non-nucleated may differ only in the detectability of their central nucleus.

Also shown in the figure is the observed mass profile of the Fornax cluster, as described in Section 4.3. The cumulative number density profile of the dwarfs matches that of the cluster mass profile very well and shows no evidence of dwarf galaxy disruption near the cluster core.

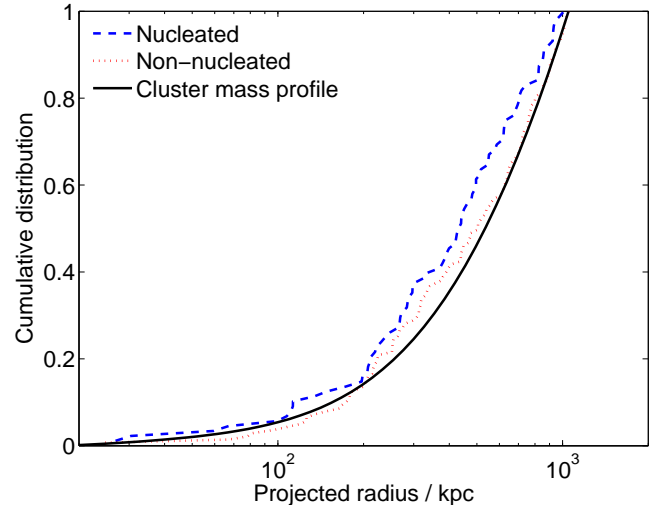


**Figure 4.** The cumulative numbers of nucleated (dashed, blue) and non-nucleated (dotted, red) dwarf galaxies in Fornax as a function of projected radius between 17.5 and 1050 kpc. Shown also as a solid, black line is the cluster mass profile described in Section 4.3.

Next, in Fig. 5 we compare the radial distributions of normal galaxies, bright and faint dwarfs and UCDs. Because the UCD survey extends only out to 314 kpc, we have adjusted the normalisation of the cumulative distribution to match that of the dwarfs at this radius.

It is immediately obvious that the different populations show different degrees of central concentration. Notably, within 314 kpc, the radial distribution of the faint dwarfs is significantly more extended than that of both the bright dwarfs and the UCDs. At first glance, this appears to be at odds with the threshing model developed below (Section 5.1). The model suggests that faint dwarfs are more compact and therefore less likely to be threshed than bright ones, but we have not looked for UCDs at magnitudes corresponding to the faint dwarfs so we cannot test the number that have been threshed. Conversely, we do not see a significant difference between the distributions of UCDs and bright dwarfs, although we would expect the UCDs to be more centrally-concentrated than the (surviving) dwarf galaxies according to our model. In this case, the relatively small number of objects involved may explain why the difference is not significant.

Outside 314 kpc the distributions of bright and faint dwarfs are indistinguishable. There are hints that the UCD distribution is flattening between 200 and 314 kpc and no UCDs have been detected in (incomplete) observations in a few fields beyond this radius. For the purposes of the modelling that follows, we therefore assume that there are no UCDs with cluster-centric radii exceeding 314 kpc. If there are any, the number density of dwarfs rises so rapidly in this region that the latter would dominate anyway.

We plot the radial distribution of normal galaxies just for interest. The numbers are so few that it is formally indistinguishable from either the bright or faint dwarf population. We note, however, that it is significantly less centrally-concentrated within 314 kpc than the UCD population.

Assuming a spherically-symmetric distribution depen-

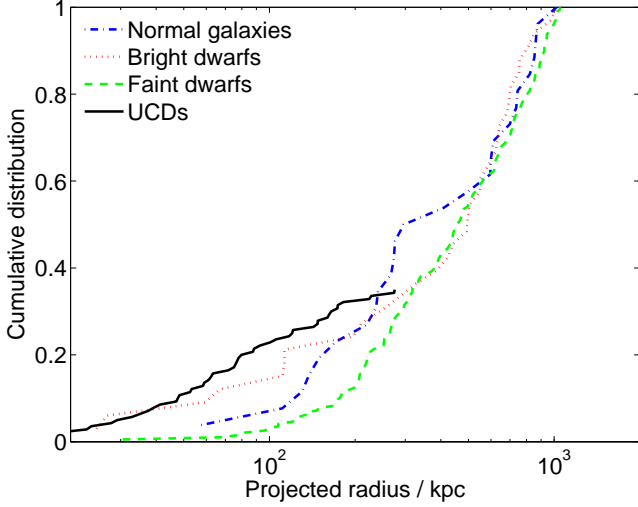


**Figure 5.** The cumulative numbers of normal galaxies (dash-dotted, blue), bright dwarfs (dotted, red), faint dwarfs (dashed, green) and UCDs (solid, black) in Fornax as a function of projected radius between 17.5 and 1050 kpc. We have adjusted the normalisation of the UCD curve to match that of the dwarfs at 314 kpc.

dent only on radius,  $r$ , we model the density,  $\rho(r)$ , with profiles of the form

$$\rho = \frac{\rho_0}{x(1+x)^{s-1}}, \quad (2)$$

where  $x = r/a$ , and  $a$  and  $s$  are fitting parameters. (We fit only for the shape of the distribution: the normalisation  $\rho_0$  can be chosen so as to match the correct number of objects.) We project each distribution onto the sky and then compare the predicted cumulative mass profile as a function of radius to the observed distribution, using a Kolmogorov–Smirnov test.

Fig. 6 shows the allowable range of parameters and Fig. 7 shows the best-fit model, although there is a strong degeneracy between  $a$  and  $s$  such that a wide variety of fits are acceptable. We will show results for  $s = 3.0$ ,  $a = 5$  kpc and for  $s = 4.0$ ,  $a = 90$  kpc; both lead to very similar conclusions.

## 4.2 Velocities

The velocity dispersions for different sub-samples of Fornax UCDs and galaxies are shown in Table 3. To determine the population velocity dispersions,  $\sigma$ , we used the following formula:

$$\sigma^2 \sum_i w_i = \sum_i w_i ((v_i - \bar{v})^2 - \sigma_{e,i}^2), \quad (3)$$

where  $v_i$  and  $\sigma_{e,i}$  are the observed velocities and their rms measurement errors, respectively,  $\bar{v}$  is the mean velocity for the full sample of all galaxies plus UCDs outside 17.5 kpc,

$$\bar{v} \sum_i w_i = \sum_i w_i v_i, \quad (4)$$

and

$$w_i = \frac{1}{\sigma^2 + \sigma_{e,i}^2} \quad (5)$$

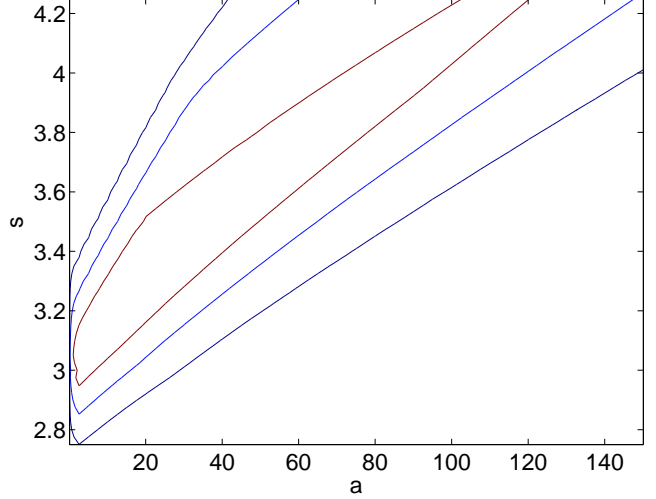


**Figure 6.** The 1-, 2-, and 3-sigma range of allowable parameters in the fit to the joint UCD plus bright dwarf population.

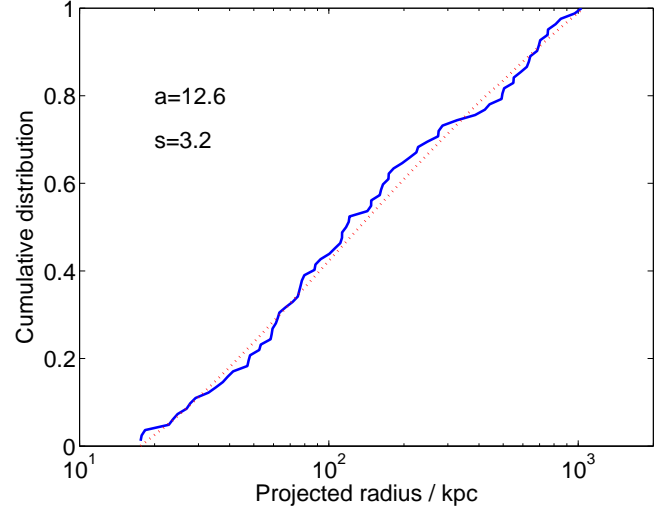


**Figure 7.** The best-fitting cumulative profile of the total number of UCD+bright dwarf galaxies as a function of projected radius: (solid, blue) data, (dotted, red) model.

are weights chosen so as to maximise the information in the data.<sup>2</sup>

The low velocity dispersion of UCDs as compared to other galaxies is expected in the threshing model, because the UCDs are more centrally-concentrated in the cluster potential (i.e. have a steeper density profile) – unfortunately there are too few UCDs to quantify this. However, the table shows a number of other features that are hard to explain.

Firstly, why is the velocity dispersion of normal galaxies so much smaller than that of dwarfs, and especially bright dwarfs, given that the two have similar radial distributions within the cluster? In Drinkwater et al. (2001a) this differ-

<sup>2</sup> We do not have any formal proof of this but note that the weights are equal when  $\sigma_{e,i} \ll \sigma$  and tend to the known optimal weighting  $w_i \propto 1/\sigma_{e,i}^2$  when  $\sigma_{e,i} \gg \sigma$  (Irwin 1942). A similar, but not identical expression is given by Pryor & Meylan (1993).

**Table 3.** Velocity dispersions for different subsamples of the UCD and galaxy populations in Fornax. The completeness of the velocity data and be found by comparing the numbers in this table with those in Table 2, but basically it is high except for the faint dwarfs. When calculating velocity dispersions for the different sub-samples, we have used the mean for the full sample of all galaxies (normal, dwarf and UCD) with radii greater than 17.5 kpc,  $\bar{v} = 1491 \text{ km s}^{-1}$ . The final column shows the rms error in the velocity dispersion measurements determined by bootstrap resampling 1000 times.

Sample	Number	$\sigma/\text{km s}^{-1}$		error
		raw	corrected	
Full	154	321	316	19
UCDs + bright dwarfs	82	316	310	27
Normal	29	281	280	40
Bright dwarfs	33	401	399	42
Faint dwarfs	43	356	350	31
UCDs	49	235	224	29
UCDs, $17.5 < R/\text{kpc} < 76$	24	285	276	42
UCDs, $76 < R/\text{kpc} < 314$	25	174	159	28

ence was interpreted as indicating that the dwarf galaxies were an unrelaxed, infalling, population. In this paper we are assuming that all galaxies (including UCDs) are relaxed: an alternative explanation is that many of the dwarfs may be orbiting in bound subhalos, with normal galaxies located at their centres.

Secondly, the line-of-sight velocity dispersion for UCDs is significantly higher at small radii than at large ones. Some difference of this kind would be expected if the UCDs are on preferentially radial orbits. Defining the velocity anisotropy parameter as  $\beta = 1 - \sigma_t^2/\sigma_r^2$ , where  $\sigma_r$  is the radial velocity dispersion with respect to the cluster centre and  $\sigma_t$  the tangential one, then this would correspond to  $\beta > 0$ . Unfortunately, the expected variation, calculated in Appendix B, is much too small to explain the observations. The observed decline in velocity dispersion between the inner and outer bin is 1:0.58. Even if we allow each measurement to move up to 1-sigma towards agreement (with probability less than 3 per cent), then the ratio remains 1:0.80. This can only be explained with  $\beta = 1$ , corresponding to purely radial orbits. The explanation for this discrepancy may be related to the non-uniform distribution of UCDs within the Fornax cluster. If the outer UCDs have orbits that are preferentially moving perpendicular to the line-of-sight, then that would explain the effect.

Despite these uncertainties, we will model the joint UCD plus bright dwarf population as if it is relaxed. As we show in the next section, this provides a marginally acceptable fit to the known mass distribution in the Fornax cluster.

### 4.3 Cluster mass profile

The mass of Fornax has been investigated using a number of different techniques that probe different radial locations. Richtler et al. (2004) look at the dynamics of the globular

cluster population around NGC 1399. They find that

$$\frac{M}{M_\odot} \approx 4.5 \times 10^{10} \frac{r}{\text{kpc}} \quad (6)$$

for  $r \lesssim 20 \text{ kpc}$  and increases in a similar vein to about twice this radius. This agrees with the ASCA observations of Ikebe et al. (1996) and the ROSAT observations of Jones et al. (1997). The two X-ray papers give different mass profiles at larger radii, but agree on a mass of  $10^{13} M_\odot$  within 200 kpc. Finally, Drinkwater et al. (2001a) have used the shape of the velocity cusp to determine a mass for the cluster as a whole of approximately  $6 \times 10^{13} M_\odot$  within 1 Mpc.

We combine all these estimates into a density/mass model consisting of an inner truncated isothermal sphere centred on NGC 1399, plus a cluster NFW potential:

$$\rho = \frac{\rho_{\text{BCG},0}}{x_{\text{BCG}}^2 (1 + x_{\text{BCG}}^2)} + \frac{\rho_{\text{clus},0}}{x_{\text{clus}} (1 + x_{\text{clus}})^2}; \quad (7)$$

$$M_r = M_{\text{BCG}} \frac{2}{\pi} \arctan x_{\text{BCG}} + M_{\text{clus},0} \left[ \ln(1 + x_{\text{clus}}) - \frac{x_{\text{clus}}}{1 + x_{\text{clus}}} \right], \quad (8)$$

where  $M_{\text{BCG}} = 2\pi^2 a_{\text{BCG}}^3 \rho_{\text{BCG},0} = 2.0 \times 10^{12} M_\odot$ ;  $a_{\text{BCG}} = 30 \text{ kpc}$ ;  $M_{\text{clus},0} = 4\pi \rho_{\text{clus},0} a_{\text{clus}}^3 = 1.1 \times 10^{14} M_\odot$ ;  $a_{\text{clus}} = 400 \text{ kpc}$ . Here  $\rho(r)$  is the density at clustocentric radius  $r$ ,  $M_r$  is the mass contained within radius  $r$ ,  $x_{\text{BCG}} = r/a_{\text{BCG}}$  and  $x_{\text{clus}} = r/a_{\text{clus}}$ . Given the uncertainties in the observations, any other model that has  $M \propto r$  in the centre, and that passes through the other mass points mentioned above, would be equally acceptable. The observational constraints are shown in Fig. 8 as black circles, and the model as a solid, magenta line.

If the joint UCD plus bright dwarf population is to be at rest in the cluster then it must satisfy the Jeans equation:

$$\frac{1}{\rho} \frac{d\rho\sigma_r^2}{dr} + \frac{2\beta\sigma_r^2}{r} = -\frac{GM_r}{r^2}. \quad (9)$$

We can use this in two ways: to predict the mass distribution, given our dynamical model for the population, or to predict the velocity dispersion profile for the given observed mass profile.

Fig. 8 shows a comparison between the observed mass profile and that predicted by two of the acceptable density models with constant velocity dispersion of  $310 \text{ km s}^{-1}$  and isotropic velocity dispersion tensors,  $\beta = 0$ . We have also tried models with  $\beta > 0$ . This makes very little difference to the  $s = 3$  prediction but substantially worsens the  $s = 4$  fit to the data at small radii.

Reversing this procedure, Fig. 9 gives the predicted velocity dispersion profile for a given density profile and observed cluster mass distribution. In making this prediction, we have taken the approximation that the logarithmic gradient in the velocity dispersion is small compared to that of the density. Once again, taking  $\beta$  to be greater than zero makes little difference to the  $s = 3$  prediction, but worsens the  $s = 4$  one, giving higher predicted velocity dispersion at small radii.

In both these plots, the  $s = 3$  curve provides the closer fit to the data. That it does not match every wiggle in the mass profile in Fig. 8 is not surprising given that the latter is somewhat arbitrary and that we have not allowed the velocity dispersion to vary with radius. The normalisation is a

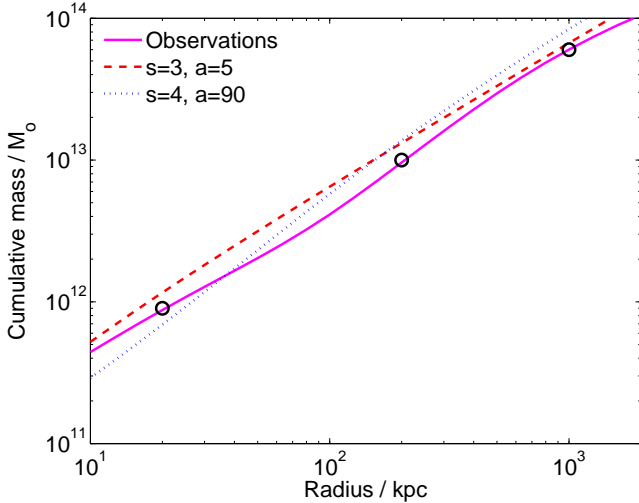


**Figure 8.** A comparison of the observed and modelled cluster mass profiles for the case of  $\beta = 0$ : observations (black circles and solid, magenta line),  $s = 3$ ,  $a = 5$  kpc (dashed, red line);  $s = 4$ ,  $a = 90$  kpc (dotted, blue line).

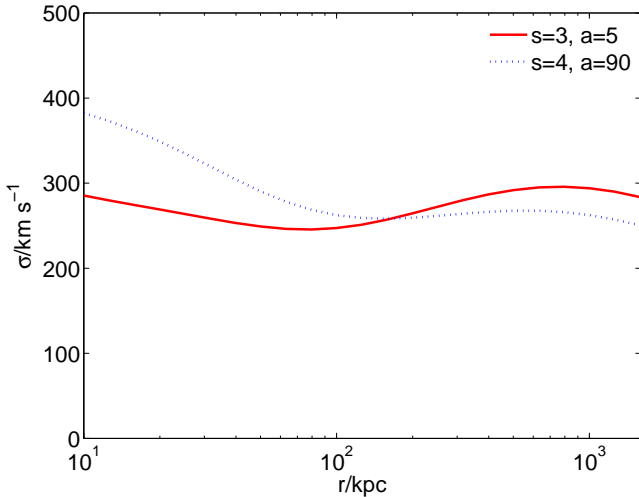


**Figure 9.** The predicted isotropic velocity dispersion profiles for the mass model given in equation 8 and for density profiles with parameters  $s = 3$ ,  $a = 5$  kpc (solid, red) and  $s = 4$ ,  $a = 90$  kpc (dotted, blue).

little too high: lowering the velocity dispersion to  $283 \text{ km s}^{-1}$  would provide a very good fit to the mass profile. Given that this is only 1-sigma away from the measured value in Table 3, we regard this as marginally acceptable.

In Fig. 9 it may seem at first sight that the decline in velocity dispersion away from the core of the cluster mimics that seen in the UCD observations. However, a closer inspection reveals that the minimum in velocity dispersion seen in this plot lies at too small a radius and that by the edge of the UCD observations at around 300 kpc the velocity dispersion has risen to its central value.

We conclude that a joint density profile for the combined UCD plus bright dwarf population of the form of equation 2 with  $s = 3$  and  $a = 5$  kpc provides an acceptable fit both to the observed UCD plus dwarf population,

in agreement with previous mass estimates of the Fornax cluster.

## 5 A STATIC MODEL OF GALAXY THRESHING

In this section, we investigate the simplest threshing scenario in which dwarf galaxies orbit within the present-day Fornax cluster and are threshed if they pass close to the cluster core. We show that there are too many UCD galaxies at large radii for this model to be viable. We conclude that in any threshing model, disruption must occur near the cores of smaller subclumps, prior to cluster formation.

### 5.1 Threshing radii

To estimate the fraction of dwarf orbits at a given radius which lead to threshing, we calculate the probability for a galaxy with initial projected clustocentric radius and line-of-sight velocity to have  $R_{\min} < R_{\text{th}}$ . Here  $R_{\min}$  is the minimum distance from the cluster center during its orbit and  $R_{\text{th}}$  is the radius within which the stellar envelope of a nucleated dwarf can be removed by the tidal field of a cluster.

To determine  $R_{\text{th}}$  for a dwarf orbiting a cluster we assume that  $R_{\text{th}}$  is the distance from the cluster center at which the tidal force of the cluster equals the self-gravitational force of the dark-matter halo in the inner regions of the dwarf galaxy. This occurs at the clustocentric radius for which

$$\frac{GM_{\text{dm}}}{r_{\text{dm}}^2} = r_{\text{dm}} \left| \frac{d}{dr} \left( \frac{GM_{\text{clus}}}{r^2} \right) \right|, \quad (10)$$

where  $M_{\text{dm}}$  is the dwarf halo mass within radius  $r_{\text{dm}}$  and  $M_{\text{clus}}$  is the cluster mass profile from equation 8.

For the dark matter distribution in dwarf galaxies we use a profile proposed by Burkert (1995):

$$\rho_{\text{dm}} = \frac{\rho_{\text{dm},0}}{(1+x_{\text{dm}})(1+x_{\text{dm}}^2)}, \quad (11)$$

where  $x_{\text{dm}} = r_{\text{dm}}/a_{\text{dm}}$ , and  $\rho_{\text{dm},0}$  and  $a_{\text{dm}}$  are the central dark matter density and the core (scale) radius, respectively. This has an extended, constant-density central region within which

$$\frac{M_{\text{dm}}}{r_{\text{dm}}^3} \approx 4.19\rho_{\text{dm},0}, \quad (12)$$

so that  $M_{\text{dm}}$  and  $r_{\text{dm}}$  cancel in equation 10 leaving only a dependence upon  $\rho_{\text{dm},0}$ . We note that the central mass profiles of dwarf galaxies are not very well known and could be more concentrated than assumed here. Were that to be the case, then the threshing radii would be reduced.

Burkert (1995) gives observed scaling relations between  $\rho_{\text{dm},0}$ ,  $a_{\text{dm}}$  and the circular velocity,  $v_{\text{dm},0}$ , at the core radius. At that radius the velocity dispersion (assumed isotropic) is approximately  $\sigma \approx v_{\text{dm},0}/\sqrt{2}$  and we assume that this is close to the observed value for the dwarf as a whole. The relevant relation is then:

$$\frac{\rho_{\text{dm},0}}{M_{\odot} \text{ pc}^{-3}} \approx 0.56 \left( \frac{\sigma}{\text{km s}^{-1}} \right)^{-1}. \quad (13)$$

For each UCD, we determine the most likely magnitude of its precursor dwarf using the relation of equation 1. We

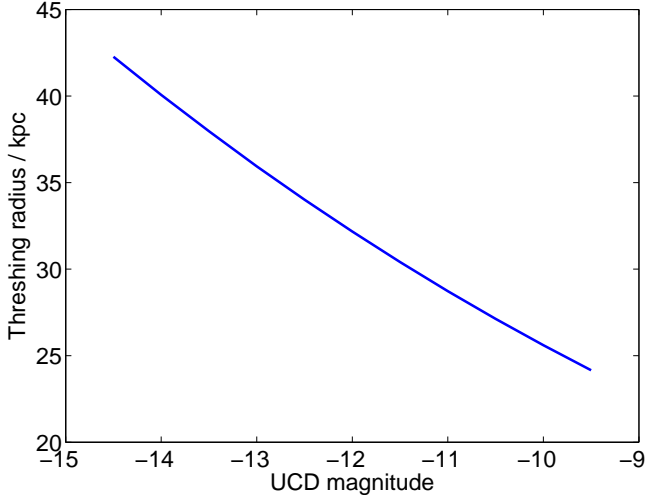


**Figure 10.** The predicted threshing radius as a function of UCD B-magnitude.

then use the observed relationship from Geha et al. (2003) to relate the magnitude to velocity dispersion,

$$\log\left(\frac{\sigma}{\text{km s}^{-1}}\right) = 0.42 - 0.07 M_B. \quad (14)$$

This fixes the mean density within the core using equation 13, and we insert this in equation 10 to determine the threshing radius of any UCD as a function of its absolute magnitude. The results of these calculations are shown in Fig. 10.

Our approach in estimating the threshing radii is very similar to that used by Bekki et al. (2003) except for the following differences. First, we specifically use the local gradient of the cluster potential (rather than the point-mass assumption) and we add a core component to the cluster NFW potential. Secondly, we have used more recent scaling relations to derive the dwarf galaxy core masses as a function of their absolute magnitudes. Our estimates give very similar threshing radii: compare our Fig. 10 with their fig. 7.

Recently, Goerdt et al. (2007, hereafter GMK07) have conducted numerical simulations of threshing in a static potential similar to that of the Virgo Cluster. They use two different models of a dwarf galaxy: one which consists solely of an extended dark matter halo with an NFW profile, and one in which this profile has been centrally-concentrated by a dissipative baryonic disk. For the latter, the threshing radii they find are similar to ours. The dark-matter-only halos can have much greater threshing radii, up to 200 kpc, but only for galaxies on quite circular orbits. As we discuss in Section 6 below, the two models bracket our predictions for UCD fractions as a function of radius, and both lead to the same qualitative results.

The detailed threshing simulations of individual dwarf galaxies by Bekki et al. (2003) showed that several pericentre passages within the threshing radius were necessary to completely strip the dwarf galaxy. In our model below we do not count the number of orbits, but simply assume that any galaxy with an orbit that passes within its threshing radius will be stripped. This assumption is reasonable for galaxies within about 100 kpc of the cluster centre, but for those galaxies with radii of order 300 kpc, on the outskirts of

the observed UCD distribution, there may have been only a single pericentric passage in the lifetime of the cluster. This could lead to an over-estimate of the UCD fraction at large radii and would strengthen our results.

## 5.2 Galaxy orbits

The equation of motion for galaxy orbits in a spherically-symmetric potential is:

$$\ddot{r} - \frac{L^2}{r^3} = -\frac{GM_r}{r^2} \quad (15)$$

where  $L = rv_t = \text{const}$  is the specific angular momentum and  $v_t$  is the tangential component of the velocity.

Combining equations 9 and 15, multiplying by  $\dot{r}$  and integrating leads to the following energy equation:

$$\frac{1}{2}\dot{r}^2 + \frac{1}{2}\frac{L^2}{r^2} - \sigma_r^2 \ln(\rho\sigma_r^2) - 2\beta\sigma_r^2 \ln r = \text{const}, \quad (16)$$

where we have taken  $\beta$  to be constant and used the approximation that the gradient in  $\sigma_r^2$  is much less than that in  $\rho$  and can be neglected. Putting in initial conditions (labelled with subscript 0) and setting  $\dot{r} = 0$ , the following equation is obtained for the minimum and maximum values of  $r$ :

$$\left(\frac{r_0}{r}\right)^2 = \left(\frac{v_0}{v_{t0}}\right)^2 + 2\left(\frac{\sigma_r}{v_{t0}}\right)^2 \left[ \ln\left(\frac{\rho}{\rho_0}\right) + \beta \ln\left(\frac{r}{r_0}\right)^2 \right]. \quad (17)$$

Simple iteration of this equation quickly finds the minimum orbital radius (pericentre).

For each value of  $r_0$ , we draw 10 000 velocities with the appropriate Gaussian distributions in each of the radial and tangential directions, then solve for the pericentric radius. An example histogram is shown in Fig. 11. The sharp spike at  $r_{\min} = r_0$  is because any orbit that has an initial radial velocity close to zero and a tangential velocity that exceeds the circular velocity at that radius will already be at pericentre. More importantly, there is a wide distribution of minimum radii extending all the way down to  $r_{\min} \approx 0$ , even for an isotropic velocity dispersion tensor. This orbital distribution is in good agreement with that found in cosmological simulations, for example by Ghigna et al. (1998).

The variation in threshing radii for different galaxies is small and so for simplicity we adopt a constant value of 30 kpc. Then for each radius,  $r$ , we can tabulate the fraction of orbits that pass within this radius. This can then be projected along the line-of-sight with the appropriate density weighting to determine the fraction of threshed orbits as a function of projected distance from the cluster centre. The results of this calculation are shown in Fig. 12 for the two example density profiles discussed above.

It is immediately apparent that the predicted fraction of threshed galaxies is far too low at radii greater than about 50 kpc. The predicted UCD fraction drops rapidly at this radius, whereas the observed fraction of UCDs stays high out to 250 kpc. (We have checked that this conclusion is unaltered even if the UCDs are distributed on a plane perpendicular to the line-of-sight such that their projected radii are equal to the true distances from the centre of the cluster.) There are many simplifications and uncertainties in the model, but it is hard to see how these could make a difference of a factor of five. The static threshing model is simply untenable.

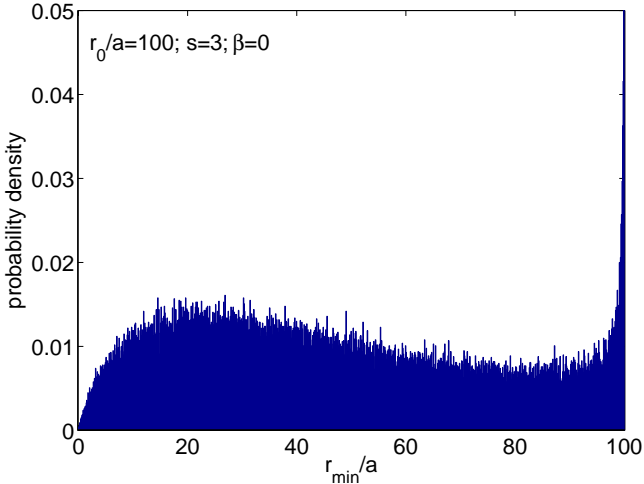


**Figure 11.** A histogram showing the probability density for the distribution of minimum orbital radii (pericentres) for a selection of galaxy orbits drawn from the appropriate Gaussian distribution of velocities. For this particular example the 1 percentile of minimum radii is at  $r_{\min} \approx 0.03 r_0$ .

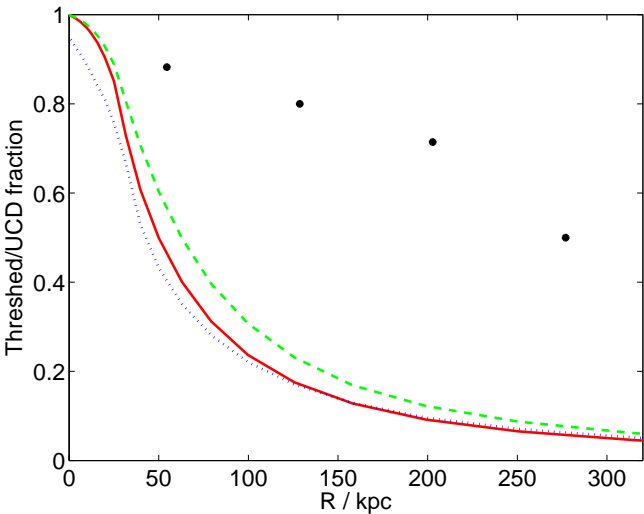


**Figure 12.** Comparison of observed and predicted fractions of UCDs. The circles show the observed UCD fraction (of the joint UCD plus bright dwarf sample) as a function of projected radius from the centre of the cluster. The lines show the predicted fraction of orbits that pass within the threshing radius of 30 kpc for  $s = 3$ ,  $a = 5$  kpc,  $\beta = 0$ , (solid, red),  $s = 5$ ,  $a = 5$  kpc,  $\beta = 0.5$ , (dashed, green), and  $s = 4$ ,  $a = 90$  kpc,  $\beta = 0.$ , (dotted, blue).

## 6 SUMMARY AND CONCLUSIONS

In this paper we have investigate the possibility that UCD galaxies are formed by the threshing of nucleated, early-type dwarf galaxies.

We first contrast the distribution of nucleated and non-nucleated dwarfs, which are indistinguishable apart from a small excess of bright, nucleated dwarfs at small cluster-centric radii. We concur with the conclusion of Côté et al. (2006) that the observations are consistent with a single population in which all dwarfs are nucleated, with a ratio of nuclear to total magnitude that varies slowly with magnitude.

However, we need to flatten their relation in order to obtain a good fit when extrapolating to fainter magnitudes.

Given this hypothesis, we can reproduce the magnitude distribution of the UCD population, except at bright magnitudes where the model predicts more UCDs than are observed. Under the threshing model, the UCDs are likely to have originated from dwarfs with magnitudes brighter than about  $M_B = -15$ . We use the joint UCD plus bright dwarf population in the modelling that follows.

The threshing model predicts that over half of all dwarf galaxies must be disrupted: 38 surviving dwarfs have nuclei of similar magnitude to the 49 observed UCDs. This may seem excessive but corresponds to an intracluster light fraction of just 8 per cent, well within the observed range for clusters of this mass (Feldmeier et al. 2004a; Feldmeier et al. 2004b; Gonzalez et al. 2005; Zibetti et al. 2005).

The distribution of dwarf galaxies in Fornax follows that of the total mass distribution and shows no evidence for disruption of dwarfs near the cluster core. Nevertheless, the UCD population is more centrally-concentrated than the dwarfs, as would be expected in the threshing model. If we assume that the joint population is in a steady-state dynamically, then it should also satisfy the Jeans Equations. We show that the joint population is well-described by a density distribution of the form

$$\rho = \frac{\rho_0}{x(1+x)^{s-1}}, \quad (18)$$

where  $x = r/a$ , and  $a$  and  $s$  are constants, with  $s$  lying between about 3 and 4.5.

The velocity dispersion of UCD galaxies shows a sharp decline with radius that is hard to explain. It may in part be due to a radial bias in the orbits, but this is not enough in itself to explain the effect. The velocity dispersion of bright dwarfs is greater than that of the UCDs. When the two are combined, then the joint population with density slope  $s = 3$  provides a marginally-acceptable fit to the mass profile of Fornax.

We have tested the simplest possible threshing model, in which dwarf galaxies move on orbits in a static cluster potential and are threshed if they pass within a radius at which the tidal force from the cluster exceeds the internal gravity at the core their dark matter halo. This fails to reproduce the observed fraction of UCDs at radii greater than 50 kpc from the core of Fornax. There are many deficiencies in the model but these are unlikely to raise the threshing radii by a factor of 5, as is required, and so we conclude that this static mode is unviable.

Our results have several points of agreement with the earlier work by Bekki et al. (2003) despite a very different approach: we have used analytic descriptions of the cluster dynamics compared to their numerical computations. In our work we have based our prediction on a parent sample of dwarf galaxies generated directly from the known Fornax galaxies, whereas Bekki et al. generated their galaxy sample from more general empirical relations for the luminosity functions and radial profiles of galaxies within clusters. In particular, they used a King profile with a core radius of 50 kpc for the density distribution, very different from our model. They demonstrate that dwarf galaxies are disrupted if they pass inside their critical threshing radius when orbiting the cluster centre. They then use this radius to estimate

the population of threshed galaxies (UCDs) in the Fornax Cluster. They find this to be consistent with the known distribution of the 7 very luminous UCDs known in the cluster at that time.

Our conclusion (refuting the simple threshing model) differs from that of Bekki et al. for a number of reasons. Firstly, we use the measured positions of galaxies in Fornax, rather than a generic King model. We also have many fewer dwarf galaxies than predicted by their Schechter model for the cluster luminosity function. In addition, we have extended the analysis to much lower luminosities of both the UCDs (as new data have become available) and the parent galaxies (due to the greater difference in nuclear to total luminosity now used). This new analysis has clearly revealed a disagreement between the number of UCDs at large clustercentric distances and the threshing predictions.

A recent paper by GMK07 undertook an extensive series of simulations to investigate the disruption of UCD host galaxies within a cluster potential similar to that of the Virgo cluster. They considered two different models for the host galaxy with very different degrees of central concentration and followed their threshing in a static potential over 5 Gyr. They then looked at the orbits of particles in a cosmological simulation of cluster formation to assess which of those orbits would lead to threshing. This latter step follows the dynamical evolution of the halo and is much more realistic than a static potential.

GMK07 state that their model “leads to the observed spatial distribution of UCDs”, in apparent disagreement with our results above. In fact our theoretical UCD fractions as a function of radius agree with theirs and are bracketed by their upper and lower predictions. The difference in the conclusion arises from the very different observed threshing fractions that we adopt. GMK07 use only 15 UCDs in both Virgo and Fornax combined, whereas we use a new sample of 49 UCDs from Fornax alone. Also, GMK07 do not say how they define the nucleated dwarfs corresponding to the parent sample, whereas we are careful to select only those dwarfs that would have nuclei that match those of the observed UCDs.

In conclusion, the origin of UCDs as dwarf galaxy nuclei remains unproven. Our modelling has revealed a number of attractive features:

The distribution of nuclear magnitudes for dwarf galaxies roughly matches that of known UCD galaxies.

UCDs are more centrally-concentrated within Fornax than are dwarf galaxies. (However, this would also be true if the UCDs constituted an extended globular cluster population around NGC 1399.)

The joint UCD plus bright dwarf population has a smooth density profile with a recognisable (NFW) form and appears to sit in dynamical equilibrium within the Fornax cluster.

At the same time, there are several major deficiencies in the model:

The model requires that more dwarf galaxies must have been disrupted in Fornax than currently remain. However, the spatial distribution of dwarfs matches that of the total mass profile of the cluster and shows no sign of galaxy disruption near the cluster core.

The very low velocity dispersion of UCDs as compared

to bright dwarfs is unexplained, as is the sharp decline in velocity dispersion of the UCDs with radius. (However, this would prove true for any dynamical model of the UCD population, regardless of its origin.)

A static threshing model for UCD formation, based upon orbits within the current cluster potential, is a hopeless failure. It predicts far too few UCDs at radii greater than about 30 kpc.

The simulations of GMK07 within an evolving cluster potential also give too few UCDs at large radii.

The balance of evidence would seem to be against the threshing model. Before dismissing the model altogether, however, we note that the threshing may have occurred within smaller sub-clusters that later fell into Fornax and have not yet reached dynamical equilibrium. This mechanism is suggested by the spatial distribution of UCDs in the Fornax Cluster: they show some association with normal galaxies and, in particular, lie in a band across the cluster (Gregg et al. 2008).

In considering the threshing hypothesis for UCD formation we should not discuss the dynamical properties of the objects in isolation from their internal properties. Evstigneeva et al. (2007) studied the stellar populations of Virgo Cluster UCDs and concluded that the Virgo UCDs have stellar populations the globular clusters of the central galaxies M87 and M49 (old ages, a range of metallicity, and supersolar alpha-abundances). On this basis, the Virgo UCD stellar populations are not consistent with simple threshing model. On the other hand, Mieske et al. (2006) found metallicities and (a range of) ages in Fornax Cluster UCDs, which are more in agreement with the hypothesis that the Fornax UCDs are threshed nuclei. A detailed analysis of the structure and colours of both Virgo and Fornax UCDs (Evstigneeva et al. 2008) concluded that their structural properties could be consistent with either globular clusters or dwarf galaxy nuclei, with the interesting observation that UCDs are about twice as extended (in effective radius) as the nuclei of dwarf galaxies at the same luminosity.

Most of these observational results, as well as our own analysis in this paper, argue against the simple threshing hypothesis for UCD formation.

## ACKNOWLEDGEMENTS

This work was initiated while PAT was a visitor to Queensland under ARC Discovery Projects Grant DP0557676, and continued whilst MJD was visiting Sussex with partial funding from PPARC Grant PP/D001579/1. We would like to thank an anonymous referee for many useful suggestions for comparison with previous work.

## REFERENCES

- Arnaboldi M., Gerhard O., Aguerri J. A. L., Freeman K. C., Napolitano N. R., Okamura S., Yasuda N., 2004, *ApJ*, 614, L33
- Bekki K., Couch W. J., Drinkwater M. J., 2001, *ApJ*, 552, L105

Bekki K., Couch W. J., Drinkwater M. J., Shioya Y., 2003, MNRAS, 344, 399

Binggeli B., Tammann G. A., Sandage A., 1987, AJ, 94, 251

Blair M., Gilmore G., 1982, PASP, 94, 742

Burkert A., 1995, ApJ, 447, L25

Côté P., et al., 2006, ApJS, 165, 57 (CPF06)

Croton D. J., et al., 2006, MNRAS, 365, 11

De Lucia G., Blaizot J., 2007, MNRAS, 375, 2

Drinkwater M. J., et al., 2000a, A&A, 355, 900

Drinkwater M. J., Jones J. B., Gregg M. D., Phillipps S., 2000b, PASA, 17, 227

Drinkwater M. J., Gregg M. D., Colless M., 2001a, ApJ, 548, L139

Drinkwater M. J., Gregg M. D., Holman B. A., Brown M. J. I., 2001b, MNRAS, 326, 1076

Drinkwater M. J., Gregg M. D., Hilker M., Bekki K., Couch W. J., Ferguson H. C., Jones J. B., Phillipps S., 2003, Natur, 423, 519

Drinkwater M. J., Gregg M. D., Couch W. J., Ferguson H. C., Hilker M., Jones J. B., Karick A., Phillipps S., 2004, PASA, 21, 375

Durrell P. R., Ciardullo R., Feldmeier J. J., Jacoby G. H., Sigurdsson S., 2002, ApJ, 570, 119

Evstigneeva E. A., Gregg M. D., Drinkwater M. J., Hilker M., 2007, AJ, 133, 1722

Evstigneeva E. A., et al., 2008, AJ, submitted

Feldmeier J. J., Ciardullo R., Jacoby G. H., Durrell P. R., 2004a, ApJ, 615, 196

Feldmeier J. J., Mihos J. C., Morrison H. L., Harding P., Kaib N., Dubinski J., 2004b, ApJ, 609, 617

Ferguson H. C., 1989, AJ, 98, 367

Ferguson H. C., Sandage A., 1989, ApJ, 346, L53

Goerdt T., Moore B., Kazantzidis S., Kaufmann T., Macci A. V., Stadel J., MNRAS, in press (astro-ph/0711.1162)

Gregg M. D., et al., 2008, AJ, submitted

Geha M., Guhathakurta P., van der Marel R. P., 2003, AJ, 126, 1794

Ghigna S., Moore B., Governato F., Lake G., Quinn T., Stadel J., 1998, MNRAS, 300, 146

Gonzalez A. H., Zabludoff A. I., Zaritsky D., 2005, ApJ, 618, 195

Hilker, M., Infante, L., Vieira, G., Kissler-Patig, M., Richtler, T. 1999, A&AS, 134, 75

Hilker, M., Baumgardt, H., Infante, L., Drinkwater, M., Evstigneeva, E., Gregg, M. 2007, A&A, 463, 119

Ikebe Y., et al., 1996, Natur, 379, 427

Irwin J. O., 1942, Journal of the Royal Statistical Society, 105, 115

Jones C., Stern C., Forman W., Breen J., David L., Tucker W., Franx M., 1997, ApJ, 482, 143

Karick A. M., Drinkwater M. J., Gregg M. D., 2003, MNRAS, 344, 188

Mieske S., Hilker M., Infante L., Jordán A., 2006, AJ, 131, 2442

Minniti D., Kissler-Patig M., Goudfrooij P., Meylan G., 1998, AJ, 115, 121

Navarro J. F., Frenk C. S., White S. D. M., 1997, ApJ, 490, 493

Phillipps S., Drinkwater M. J., Gregg M. D., Jones J. B., 2001, ApJ, 560, 201

Pryor C., Meylan G., 1993, ASPC, 50, 357

**Table A2.** The UCD sample.

X	Y	R	cz	err	$M_B$
kpc	kpc	kpc	km/s	km/s	mag
-8.6	4.3	9.7	1398	77	-10.3
-0.2	-10.3	10.3	1460	77	-10.2
9.3	-6.6	11.5	1365	56	-10.5
0.1	11.7	11.7	1491	73	-10.6
9.5	7.4	12.0	1377	85	-10.3
12.3	-0.5	12.3	1445	86	-9.9
-12.5	-3.8	13.0	1332	63	-10.0
13.3	-0.2	13.3	1230	112	-10.5
-8.5	10.4	13.4	1357	148	-10.8
-4.7	-14.0	14.7	1158	64	-10.2
-14.8	4.0	15.3	1125	101	-10.8
-17.5	1.7	17.6	1377	96	-9.8
16.8	-5.9	17.7	1574	117	-10.3
-2.7	-18.1	18.3	1475	72	-10.2
-21.6	7.3	22.8	1702	55	-10.8
0.1	23.7	23.7	1607	47	-10.9
-22.1	16.9	27.8	1549	64	-11.2
-26.9	-11.4	29.2	1312	57	-12.5
-28.3	16.6	32.9	1212	32	-11.9
-26.6	23.0	35.2	1510	64	-10.8
-13.5	-35.1	37.6	1490	69	-10.5
15.4	-36.1	39.3	1980	88	-11.5
-6.8	40.7	41.3	1370	64	-10.6
25.7	-39.5	47.1	1744	89	-10.9
19.9	-43.3	47.6	1845	87	-10.7
29.7	-38.0	48.3	1591	36	-13.6
-23.3	-47.1	52.6	1764	52	-9.9
-52.0	-11.7	53.3	1641	63	-10.4
57.7	8.8	58.4	1022	46	-10.5
-53.8	24.1	59.0	1326	82	-11.2
-54.5	28.0	61.3	1146	86	-10.6
-4.1	-62.3	62.4	1698	52	-10.8

Richtler T., et al., 2004, AJ, 127, 2094

Springel V., et al., 2005, Natur, 435, 629

Zibetti S., White S. D. M., Schneider D. P., Brinkmann J., 2005, MNRAS, 358, 949

## APPENDIX A: TABLES OF GALAXY AND UCD DATA

### APPENDIX B: VARIATION IN LINE-OF-SIGHT VELOCITY WITH RADIUS.

This appendix calculates the expected variation in the line-of-sight velocity dispersion of UCDs with radius resulting from anisotropic motions in a declining density profile.

We take the velocity dispersion tensor to be aligned with the radial direction and to have diagonal components  $\sigma_r$ ,  $\sigma_t$  &  $\sigma_z$ , where  $\sigma_r$  and  $\sigma_t$  are the radial and tangential components of velocity dispersion, respectively. The velocity anisotropy parameter is defined as  $\beta = 1 - \sigma_t^2/\sigma_r^2$ —thus  $\beta = 0$  for isotropic orbits and  $\beta > 0$  for preferentially radial orbits. We assume that both  $\sigma_r^2$  and  $\beta$  are constant throughout the cluster. In practice one might expect some radial variation in these quantities, but the data are insufficient to constrain more complex models.

The line-of-sight velocity dispersion  $\sigma_{los}$  at a given projected radius  $R$  is then given by a density-weighted integral

Table A1. The galaxy sample.

FCC	X kpc	Y kpc	R kpc	cz km/s	err km/s	ref	$M_B$ mag	nuc	late	dwarf	morph
1	-1968.9	709.2	2070.2	-	-	-	-12.8	1	0	1	dE,N
2	-1656.6	666.0	1767.9	4540	9	1	-16.2	0	1	1	d:SBc(LSB)
3	-1532.9	-32.6	1534.0	1567	1	1	-17.2	0	1	0	SBcdII-III
4	-1446.4	-593.1	1577.8	-	-	-	-14.3	0	0	1	dE2
5	-1441.4	-459.9	1524.4	-	-	-	-14.0	0	0	1	dE5/ImV
6	-1460.3	-70.7	1463.6	-	-	-	-15.3	0	0	1	dE5
7	-1399.5	-33.7	1400.6	-	-	-	-12.4	0	0	1	dE1
8	-1427.5	741.2	1592.6	-	-	-	-12.8	0	0	1	dE?
9	-1400.7	976.0	1688.6	1751	3	1	-16.0	0	1	0	Sd?
10	-1392.4	1041.2	1719.4	1451	3	1	-16.8	0	1	0	Sd(onedge)
11	-1297.6	306.7	1326.5	-	-	-	-14.3	1	0	1	dE4,N
12	-1292.1	752.2	1480.9	-	-	-	-14.3	0	1	0	BCDorS
13	-1215.2	-589.4	1362.5	1792	25	2	-19.3	0	1	0	SBcII
14	-1215.9	-285.3	1254.9	1805	10	1	-13.7	0	0	1	dE3
15	-1224.6	696.6	1396.3	-	-	-	-14.7	0	0	1	dE7
16	-1184.2	-166.2	1199.2	-	-	-	-13.5	0	0	1	dE2
17	-1176.6	604.5	1312.0	-	-	-	-13.3	1	0	1	dE3,N
18	-1156.8	112.9	1159.9	-	-	-	-15.8	0	1	0	SmIII
19	-1116.3	-679.7	1319.0	1497	47	2	-16.1	1	0	1	ds0(8),N
20	-1111.8	-600.5	1274.4	-	-	-	-12.8	0	0	1	filament
21	-1096.7	-614.3	1268.0	1751	13	3	-21.9	0	0	0	S0(pec)
22	-1095.5	-577.5	1248.7	1979	11	3	-19.4	0	1	0	Sappec
23	-1051.9	-501.7	1174.2	-	-	-	-12.7	1	0	1	ImVordE5,N
25	-1040.3	-534.9	1178.8	-	-	-	-13.6	1	0	1	dE0,N
26	-1052.2	-114.7	1060.5	1786	28	3	-16.3	0	0	0	SB0(8)
27	-1042.7	223.9	1062.4	-	-	-	-12.0	0	0	1	dE2
28	-1009.1	-718.8	1250.0	1408	23	3	-17.7	0	1	0	SmIII
29	-1020.8	-354.5	1086.8	1368	26	3	-19.5	0	1	0	SBa(r)
30	-1004.3	-619.8	1190.0	-	-	-	-12.4	0	0	1	dEordS0
31	-1010.8	65.4	1011.8	1542	42	3	-14.5	0	0	1	dE4
32	-967.6	5.2	967.5	1342	27	3	-15.9	0	0	1	dEpec/BCD
33	-941.4	-544.3	1095.6	1990	14	3	-17.1	0	1	0	SdIIIpec/BCD
34	-958.4	78.7	960.3	-	-	-	-12.9	0	0	1	dE
35	-935.8	-515.7	1076.2	1841	22	3	-16.0	0	1	0	SmIV/BCD?
36	-973.0	889.3	1307.5	-	-	-	-15.4	1	0	1	dE4pec,N
37	-936.9	-319.4	994.9	1924	65	3	-17.5	0	1	0	SBcIII(interacting)
38	-934.1	-385.0	1016.4	-	-	-	-13.8	0	0	1	dEOpec
39	-924.1	-326.2	985.1	1007	18	3	-15.8	0	1	0	SdIII(interacting)
40	-913.8	-451.8	1026.2	-	-	-	-13.7	0	0	1	dE4
41	-943.4	869.1	1272.7	-	-	-	-13.7	0	1	1	ImVordE3
42	-903.0	-20.7	903.5	-	-	-	-13.0	0	0	1	dE0
43	-911.7	892.0	1265.9	1323	17	2	-17.8	1	0	1	ds0/2(5),N
44	-882.0	112.2	887.3	1232	32	3	-13.8	0	0	1	ds0
45	-879.7	312.9	929.1	-	-	-	-11.8	0	1	1	ImV
46	-839.4	-585.5	1030.9	2255	27	3	-15.7	0	0	1	dE4
47	-846.6	-91.9	852.9	1434	10	3	-18.0	0	0	0	E4
48	-846.1	314.8	898.4	1439	45	3	-14.2	0	0	1	dE3
49	-816.1	-645.3	1048.1	-	-	-	-12.1	0	0	1	dE4
50	-822.6	-23.8	823.2	-	-	-	-14.7	1	0	1	dE0,N
51	-810.3	-470.7	943.2	-	-	-	-12.8	0	0	1	dE4
52	-817.1	366.7	890.9	-	-	-	-12.8	0	0	1	dE1
53	-816.0	685.8	1058.6	1675	35	3	-16.6	0	1	0	ScdIII
54	-819.1	842.9	1167.3	-	-	-	-13.3	1	0	1	dE1,N
55	-804.0	322.6	862.1	1252	10	3	-17.4	1	0	0	S0(9),N
56	-783.9	-243.0	823.9	-	-	-	-13.8	1	0	1	dE1,N
57	-778.7	-165.2	798.2	-	-	-	-13.5	0	0	1	dE6(boxy)pec
58	-754.9	-717.1	1048.6	-	-	-	-13.3	0	0	1	dE2
59	-777.3	658.1	1011.9	-	-	-	-11.9	1	0	1	dE0,N
60	-733.8	-672.1	1001.9	-	-	-	-12.9	0	0	1	ImVordE2
61	-761.3	623.6	977.8	-	-	-	-	-	-	-	-

**Table A1** – *continued*

FCC	X kpc	Y kpc	R kpc	cz km/s	err km/s	ref	$M_B$ mag	nuc	late	dwarf	morph
	-	-13.3	1	0	1	dE3,N					
62	-731.2	-593.1	947.8	1878	30	3	-18.7	0	1	0	SbcII
63	-765.2	1104.5	1335.8	1354	19	1	-18.6	0	0	0	E4
64	-715.7	-1078.8	1302.8	-	-	-	-13.8	0	0	1	dE5
65	-739.3	74.6	742.1	-	-	-	-13.8	1	0	1	dE6,NordS0
66	-726.8	599.0	936.1	-	-	-	-14.4	0	0	1	dE3
67	-689.8	94.3	695.0	1400	21	3	-18.3	0	1	0	Sc(onedge)
68	-697.1	560.0	889.0	2030	26	3	-14.8	1	0	1	dE5,N
69	-669.4	-344.6	756.6	-	-	-	-12.6	0	0	1	ImVordE0
70	-655.7	-666.9	940.9	-	-	-	-12.8	1	0	1	dE2,N?
71	-641.8	-53.5	644.6	-	-	-	-10.8	0	0	1	dE2
72	-631.3	-145.7	649.5	-	-	-	-12.0	0	0	1	dE0/ImV
73	-623.3	-437.3	765.5	-	-	-	-11.9	0	0	1	dE3
74	-650.4	1217.1	1374.0	-	-	-	-13.6	0	0	1	dE
75	-629.6	17.6	629.6	-	-	-	-11.5	0	0	1	dE3
76	-637.1	660.8	913.0	1868	42	3	-16.6	0	1	1	ImII/dS0(6)emission
77	-618.4	-269.2	677.2	-	-	-	-13.1	1	0	1	dE0,N
78	-620.8	25.1	621.1	-	-	-	-12.1	0	0	1	ImVordE
79	-616.1	-211.6	653.7	-	-	-	-12.6	0	0	1	dE?
80	-614.7	1038.6	1201.5	-	-	-	-15.7	0	0	1	dEordS0
81	-603.7	613.3	856.2	1893	36	3	-14.2	1	0	1	dE1,N
82	-575.2	415.5	706.2	1157	50	4	-14.9	1	0	1	dE1,N
83	-565.5	207.7	600.5	1431	11	3	-19.0	0	0	0	E5
84	-562.5	142.7	578.9	-	-	-	-11.8	1	0	1	dE0,N?
85	-547.6	-34.6	549.1	1673	69	4	-15.0	1	0	1	dE0,N
86	-548.4	33.5	549.1	-	-	-	-13.8	1	0	1	dE5,N?
87	-548.6	660.9	855.0	-	-	-	-12.7	0	0	1	dE3
88	-534.0	635.5	826.3	1829	13	3	-19.5	0	1	0	SBb(r)I
89	-531.2	770.3	931.8	-	-	-	-13.3	1	0	1	dE,N
90	-516.8	-293.2	596.5	1813	15	2	-16.3	0	0	0	E4pec
91	-529.9	1185.8	1294.6	1590	12	1	-14.3	0	1	1	ImV
92	-515.1	171.0	541.3	-	-	-	-12.3	0	0	1	ImVordE
93	-505.1	-128.9	522.4	-	-	-	-11.9	0	0	1	dE2
94	-507.9	167.1	533.3	-	-	-	-12.0	0	0	1	dE0
95	-503.3	41.7	504.7	1276	12	3	-16.7	0	0	1	dSB0ordSBa
96	-491.3	-754.7	904.4	-	-	-	-12.1	0	0	1	dE0/ImV
97	-499.9	-15.4	500.2	-	-	-	-12.3	0	0	1	dE1
98	-480.6	-288.4	562.6	-	-	-	-13.1	0	0	1	ImVordE1
99	-485.3	388.2	618.9	-	-	-	-14.2	0	0	1	dE4
100	-477.9	139.2	496.6	1660	31	2	-15.8	1	0	1	dE4,N
101	-475.1	-78.7	482.2	1051	55	3	-14.1	1	0	1	dE0,NorS
102	-443.8	-268.9	520.8	1723	61	2	-14.8	0	1	1	ImIV
103	-426.8	-113.5	442.4	-	-	-	-12.0	0	0	1	dE2
104	-430.6	384.8	575.4	-	-	-	-12.8	0	0	1	dE6
105	-422.0	-222.7	478.6	-	-	-	-14.0	1	0	1	dE1,N?
106	-410.3	423.0	587.2	2066	11	3	-16.2	1	0	1	d:S0(6),N
107	-395.0	-832.9	924.5	-	-	-	-14.3	1	0	1	dE3,N?
108	-399.6	-245.3	470.4	-	-	-	-12.2	0	0	1	dE0
109	-394.0	-765.0	863.1	-	-	-	-13.0	0	0	1	dE4
110	-391.6	-100.3	404.9	-	-	-	-14.5	0	0	1	dE4
111	-393.6	602.5	717.4	1283	115	4	-14.5	1	0	1	dE0,N
112	-381.0	-346.6	516.9	-	-	-	-14.2	1	0	1	dS0(5),N
113	-384.7	223.9	443.9	1416	20	3	-16.1	0	1	0	ScdIIIpec
114	-379.7	18.6	380.1	-	-	-	-11.6	0	0	1	dE1?
115	-377.6	-93.5	389.6	1686	25	3	-14.7	0	1	0	Sdm(onedge)
116	-371.9	-197.9	422.5	1204	57	3	-15.2	1	0	1	dE1,N
117	-361.0	-827.6	905.2	-	-	-	-13.1	0	0	1	dE0
118	-357.1	347.3	496.6	-	-	-	-13.7	1	0	1	dE0,N
119	-357.6	655.3	744.7	1417	18	3	-16.3	0	0	0	S0pec
120	-344.1	-403.2	531.8	887	6	1	-15.0	0	1	1	ImIV

Table A1 – continued

FCC	X kpc	Y kpc	R kpc	cz km/s	err km/s	ref	$M_B$ mag	nuc	late	dwarf	morph
121	-343.8	-241.2	421.2	1446	12	2	-21.1	0	1	0	SBbc(s)I
122	-351.8	1056.1	1111.3	-	-	-	-14.0	0	0	1	dS0
123	-336.9	-143.0	366.8	940	21	3	-13.4	0	1	1	ImV
124	-336.9	447.1	558.2	-	-	-	-13.3	0	0	1	dE3+ImV
125	-330.7	-134.6	357.8	-	-	-	-12.6	0	0	1	dE4
126	-328.6	385.3	504.9	-	-	-	-10.9	0	0	1	dE0
127	-312.3	60.6	317.8	-	-	-	-11.5	0	0	1	dE3?
128	-306.4	-354.5	469.8	-	-	-	-14.5	0	1	1	ImIV
130	-307.5	-23.2	308.5	-	-	-	-13.1	0	1	1	ImV?
131	-305.1	77.6	314.3	-	-	-	-11.0	0	0	1	dE3
132	-295.7	-120.2	319.8	1883	98	4	-12.8	0	0	1	dE2
133	-295.1	30.8	296.5	-	-	-	-13.8	1	0	1	dE0,N
134	-296.0	299.4	419.9	1381	19	3	-13.7	1	0	1	dE5pec,NorE
135	-286.1	402.4	492.6	1232	18	3	-15.8	1	0	1	dS0(5),N
136	-283.4	-33.5	285.5	1206	23	3	-16.5	1	0	1	dE2,N
137	-265.0	-143.5	302.0	-	-	-	-14.4	1	0	1	dE0,N
138	-254.9	-304.7	398.2	-	-	-	-12.7	0	0	1	dE2
139	-259.2	981.1	1013.8	1752	24	2	-16.9	0	1	0	SBmIII
140	-252.6	90.5	267.9	-	-	-	-12.3	1	0	1	dE4,N
142	-250.9	142.4	287.9	-	-	-	-12.8	1	0	1	dE2,N
143	-249.4	97.6	267.5	1356	10	3	-17.0	0	0	0	E3
144	-247.7	44.7	251.5	-	-	-	-12.1	0	0	1	dE0
145	-241.7	81.0	254.7	-	-	-	-11.7	0	0	1	dE0
146	-234.3	44.4	238.3	-	-	-	-11.8	1	0	1	dE4,N
147	-228.2	77.8	240.8	1340	12	3	-19.4	0	0	0	E0
148	-228.1	64.1	236.6	749	10	3	-17.7	0	0	0	S0(cross)
149	-217.6	-223.8	312.8	-	-	-	-11.4	0	0	1	dE
150	-216.6	-318.8	386.1	1411	18	3	-15.6	1	0	1	dE4,N
151	-215.5	-254.2	334.0	-	-	-	-13.3	1	0	1	dE0,N?
152	-215.7	1042.5	1063.9	1389	12	2	-17.2	0	1	0	S0/apec;emission
153	-213.4	350.2	409.4	1589	10	3	-18.3	0	0	0	S0(9)
154	-212.0	69.5	222.8	-	-	-	-12.1	0	0	1	dE3
155	-209.0	225.4	306.8	-	-	-	-13.0	0	0	1	dE2
156	-197.2	39.2	200.9	-	-	-	-14.1	0	0	1	dE1
157	-196.7	-22.2	198.0	-	-	-	-13.0	1	0	1	dE0,N?
158	-191.4	-188.3	268.9	-	-	-	-14.5	1	0	1	dE6,N
159	-183.0	217.3	283.7	-	-	-	-13.2	1	0	1	dE3,N
160	-171.9	21.5	173.1	-	-	-	-13.6	1	0	1	dE1,N
161	-171.7	2.6	171.7	1351	10	3	-19.6	0	0	0	E0
162	-167.8	5.9	167.9	-	-	-	-11.3	0	0	1	dE0
163	-167.5	-137.0	216.7	-	-	-	-11.5	0	0	1	dE0
164	-159.8	-250.0	297.1	1427	49	3	-14.9	1	0	1	dS0(5),N
165	-147.7	-160.9	218.8	-	-	-	-13.8	0	0	1	dE6
166	-144.9	-598.1	615.8	-	-	-	-13.2	1	0	1	dE3,N
167	-144.6	165.3	219.4	1953	13	2	-20.0	0	0	0	S0/a
168	-143.9	83.7	166.3	-	-	-	-12.6	0	0	1	dE0
169	-140.6	226.2	266.1	-	-	-	-14.1	0	0	1	dE2
170	-139.2	53.6	149.1	1744	10	3	-18.3	0	0	0	S0(9)(boxy)
171	-132.2	22.5	134.0	-	-	-	-13.4	1	0	1	dE0,N?
172	-129.8	-668.4	681.1	-	-	-	-10.9	0	0	1	dE4
173	-127.4	450.7	468.1	-	-	-	-13.3	0	0	1	dE3/ImV
174	-126.3	850.6	859.7	1801	46	3	-14.6	1	0	1	dE1,NorE(cD)
175	-125.8	5.2	125.9	-	-	-	-12.5	0	0	1	dE3
176	-121.8	-281.3	306.8	1410	10	3	-17.6	0	1	0	SBa(s)
177	-121.3	248.3	276.1	1558	9	3	-18.1	0	0	0	S0(9)(cross)
178	-120.6	408.5	425.7	-	-	-	-14.1	1	0	1	dE3,N
179	-120.7	-192.1	227.1	908	27	3	-18.9	0	1	0	Sa
180	-117.0	-272.0	296.3	-	-	-	-13.3	0	0	1	dS0
181	-114.2	178.8	212.0	1113	53	2	-14.1	1	0	1	dE2,N
182	-112.2	26.5	115.3	1669	11	3	-16.4	0	1	0	Sa0

**Table A1** – *continued*

FCC	X kpc	Y kpc	R kpc	cz km/s	err km/s	ref	$M_B$ mag	nuc	late	dwarf	morph
183	-112.4	-361.6	378.9	-	-	-	-14.1	1	0	1	dS0(7),N
184	-108.9	-20.1	110.8	1257	12	2	-19.0	0	0	0	SB0
185	-102.9	200.7	225.4	-	-	-	-11.8	0	0	1	dE3
186	-103.7	-937.0	942.9	-	-	-	-13.5	0	0	1	dE4
187	-100.7	295.7	312.3	-	-	-	-13.8	0	0	1	dE5
188	-99.8	-48.8	111.1	1046	43	3	-15.2	1	0	1	dE0,N
190	-95.1	89.1	130.1	1770	10	3	-17.8	0	0	0	SB0
191	-93.6	22.2	96.2	-	-	-	-12.0	0	0	1	dE3
192	-93.0	-152.8	179.0	-	-	-	-11.7	0	0	1	dE0
193	-91.1	-103.1	137.7	905	10	3	-18.5	0	0	0	SB0(5)
194	-83.9	-86.7	120.7	1237	84	4	-13.1	0	0	1	dE3
195	-78.3	192.1	207.3	1315	69	4	-14.6	1	0	1	dE5,N
196	-64.9	-132.2	147.4	1797	129	4	-13.6	0	0	1	dE6
197	-57.0	53.8	78.3	-	-	-	-12.2	0	0	1	dE3
198	-53.6	-613.9	616.2	-	-	-	-13.4	0	0	1	dE5
199	-52.8	-445.5	448.7	-	-	-	-12.3	0	1	1	ImV
200	-40.8	198.4	202.5	1184	110	4	-13.9	0	0	1	dE2
201	-40.9	-638.6	640.0	1922	126	2	-14.6	0	0	1	dE4
202	-26.6	3.7	26.9	825	20	3	-16.0	1	0	1	d:E6,N
203	-23.7	325.3	326.2	1124	16	3	-15.8	1	0	1	dE6,N
204	-18.6	811.1	811.3	1364	26	3	-16.4	1	0	1	dS0(8),N
205	-24.9	-923.4	923.7	1450	27	3	-14.4	1	0	1	dE1,N?
206	-17.9	-642.1	642.4	1402	20	2	-15.5	0	0	1	dE0pec
207	-11.6	112.2	112.9	1403	20	3	-15.4	1	0	1	dE2,N
208	-12.0	-28.0	30.5	1720	50	1	-14.0	1	0	1	dE2,N
209	-7.9	625.0	625.0	-	-	-	-12.6	1	0	1	dE5,N
210	-11.5	-214.8	215.2	-	-	-	-12.6	0	0	1	dE0
211	-8.9	66.6	67.1	2260	22	3	-15.0	1	0	1	d:E2,N
212	-9.4	-336.2	336.3	-	-	-	-13.7	0	0	1	dE1?
213	0.3	-0.6	0.7	1440	19	3	-20.7	0	0	0	E0
214	9.0	-133.9	134.2	-	-	-	-12.3	0	0	1	dE0
215	10.2	-107.0	107.5	-	-	-	-12.1	1	0	1	dE,N?
216	12.0	-386.7	386.8	-	-	-	-12.1	0	0	1	dE0
217	14.7	-445.7	445.9	-	-	-	-11.6	0	0	1	dE/ImV
218	19.5	64.4	67.3	-	-	-	-12.8	0	0	1	dE4
219	27.5	-50.6	57.5	1919	15	3	-20.4	0	0	0	E2
220	31.1	74.6	80.8	-	-	-	-11.8	0	0	1	dE2
221	43.2	-226.3	230.5	1724	77	4	-13.6	1	0	1	dE4,N
222	52.7	27.7	59.5	792	26	3	-15.7	1	0	1	dE0,N
223	59.8	-95.8	113.0	781	62	3	-15.1	1	0	1	dE0,N
224	78.9	1277.2	1279.5	-	-	-	-14.4	0	0	1	ImVordE
225	80.3	-385.1	393.5	-	-	-	-11.7	0	0	1	dE4
226	96.8	149.3	177.8	-	-	-	-13.5	0	0	1	dE?
227	96.2	-25.2	99.4	-	-	-	-12.0	1	0	1	dE0,N?
228	97.8	44.8	107.5	-	-	-	-12.5	0	0	1	dE0
229	102.0	-74.0	126.1	-	-	-	-12.2	0	0	1	dE0
230	110.3	241.7	265.5	1088	30	3	-14.1	1	0	1	dE5,N
231	115.1	447.8	462.1	-	-	-	-12.9	1	0	1	dE0,N?
232	121.0	1093.0	1099.5	-	-	-	-13.9	1	0	1	dE7,N
233	114.1	-273.4	296.5	-	-	-	-11.7	0	1	1	ImV
234	121.2	350.5	370.7	-	-	-	-14.1	1	0	1	dE5,N
235	118.6	-60.8	133.4	1974	20	2	-17.9	0	1	1	ImIII
236	119.0	-134.7	180.0	-	-	-	-12.1	0	0	1	dE2
237	133.6	708.2	720.4	-	-	-	-13.5	0	0	1	dE3
238	126.4	-378.6	399.5	-	-	-	-12.6	1	0	1	dE5,N
239	126.5	-715.4	726.8	-	-	-	-12.4	0	0	1	dE5
240	146.7	1314.3	1322.1	-	-	-	-14.8	0	1	1	ImIV
241	135.9	60.9	148.8	-	-	-	-14.7	1	0	1	dE0,N
242	128.7	-765.8	776.9	-	-	-	-13.5	0	0	1	dE5
243	138.0	-366.1	391.6	1404	45	2	-14.8	1	0	1	dE1,N

Table A1 – continued

FCC	X kpc	Y kpc	R kpc	cz km/s	err km/s	ref	$M_B$ mag	nuc	late	dwarf	morph
244	143.5	-149.2	207.2	831	108	4	-13.1	0	0	1	dE6/ImIV?
245	148.7	149.3	210.4	2187	25	3	-15.3	1	0	1	dE0,N
246	151.2	-234.1	279.0	-	-	-	-12.2	0	0	1	dE2
247	157.6	-73.6	174.1	1097	108	4	-13.5	0	0	1	dE3/Im?
248	158.5	-143.3	214.0	-	-	-	-12.6	0	0	1	dE3
249	153.5	-719.2	735.9	1533	10	3	-17.7	0	0	0	E0
250	156.4	-683.4	701.5	-	-	-	-14.2	0	0	1	dE1
251	167.5	149.0	223.9	-	-	-	-12.3	0	0	1	dE0
252	166.9	-104.0	196.9	1415	35	2	-15.3	1	0	1	dE0,N
253	168.1	-833.5	850.8	1677	57	2	-15.0	1	0	1	dE5,N?
254	179.2	-101.8	206.4	1517	94	4	-13.7	1	0	1	dE0,N
255	186.9	583.5	612.2	1271	10	3	-17.6	1	0	0	S0(6),N
256	184.5	173.1	252.6	-	-	-	-11.2	0	0	1	dE3
258	186.8	-83.7	205.0	-	-	-	-11.7	0	0	1	dE2
259	187.6	-22.5	189.0	-	-	-	-13.5	0	0	1	dE2
260	194.8	101.9	219.5	1493	59	3	-14.3	1	0	1	dE0,N
261	208.6	586.8	622.1	1492	42	2	-15.5	1	0	1	dE3pec,N/ImI
262	203.0	-173.9	267.8	-	-	-	-13.5	0	0	1	dE1
263	218.8	195.8	293.0	1733	8	4	-16.7	0	1	0	SBcdIII
264	216.3	-48.5	221.8	1888	43	3	-14.5	1	0	1	dS0(8),N
265	234.9	686.3	724.5	-	-	-	-13.2	0	0	1	dE5
266	228.6	97.8	248.3	1551	39	4	-15.4	1	0	1	dE0,N
267	237.6	579.1	625.1	834	10	2	-15.3	0	1	0	SmIV
268	234.5	-411.8	474.7	-	-	-	-13.0	0	0	1	dE1
269	247.4	55.2	253.3	-	-	-	-13.0	0	0	1	dE0
270	243.1	-762.3	801.2	-	-	-	-11.6	0	0	1	dE
271	259.3	209.7	332.8	-	-	-	-12.6	0	0	1	dE1
272	263.1	2.3	263.1	-	-	-	-12.1	0	0	1	dE
273	272.0	347.5	440.2	-	-	-	-12.5	0	0	1	dE2
274	270.2	-31.5	272.2	950	45	3	-14.8	1	0	1	dE0,N
275	272.1	-38.6	275.0	-	-	-	-12.0	0	0	1	dE
276	273.1	19.4	273.7	1382	12	4	-19.5	0	0	0	E4
277	278.0	103.4	296.1	1613	25	4	-17.5	0	0	0	E5(boxy)
278	287.8	551.4	620.7	2125	30	2	-14.5	1	0	1	dE6,N
279	276.9	-431.7	514.1	-	-	-	-14.6	1	0	1	dE0,N
280	291.9	-176.5	341.9	-	-	-	-12.7	0	0	1	dE1
281	294.3	-145.7	329.1	-	-	-	-13.4	0	0	1	dE1
282	309.6	534.2	616.0	1251	19	3	-16.8	0	1	1	ImIV/dEpec;emission
283	286.1	-970.4	1013.2	-	-	-	-13.5	0	0	1	dE2
284	315.5	37.4	317.5	-	-	-	-12.3	0	0	1	dE1
285	320.1	-286.6	430.9	891	6	2	-17.1	0	1	0	SdIII?
286	339.5	281.8	439.9	1673	82	3	-13.2	1	0	1	dE0,N?
288	354.5	527.6	633.9	1088	20	3	-15.9	1	0	1	dS0(9),N
289	351.8	263.6	438.3	-	-	-	-12.6	0	0	1	dE0
290	363.2	-141.2	390.6	1366	12	3	-18.5	0	1	0	ScII
291	369.2	81.9	377.7	-	-	-	-11.9	0	0	1	dE5
292	396.8	840.9	927.5	-	-	-	-14.2	1	0	1	dE6,N?
293	419.9	-141.8	444.2	-	-	-	-13.7	1	0	1	dE1,N
294	423.4	-75.2	430.5	-	-	-	-14.1	1	0	1	dE1,N?
295	429.1	94.9	438.9	-	-	-	-12.4	0	0	1	dE0
296	432.6	88.8	440.9	856	41	3	-15.0	1	0	1	dE1,N
297	435.8	-185.8	475.1	-	-	-	-13.5	0	0	1	dE1
298	443.5	-81.4	451.5	1620	31	3	-14.7	1	0	1	dE2,N
299	453.3	-504.2	680.8	2151	40	2	-14.2	0	1	0	Sd(onedge)
300	458.2	-303.4	551.6	-	-	-	-15.2	1	0	1	dE4,N
301	464.6	-182.4	500.5	1038	13	3	-17.1	0	0	0	E4
302	477.2	-42.0	479.3	806	23	2	-15.6	0	1	0	Sdm(onedge)
303	471.0	-518.9	703.8	1980	31	2	-15.8	1	0	1	dE1,N
304	505.6	329.9	601.3	-	-	-	-12.5	0	0	1	dE1

**Table A1** – *continued*

FCC	X kpc	Y kpc	R kpc	cz km/s	err km/s	ref	$M_B$ mag	nuc	late	dwarf	morph
305	493.0	-569.8	756.9	1228	25	2	-15.6	0	0	1	dS0(6)
306	511.3	-312.7	601.8	898	14	2	-15.7	0	1	0	SBmIII
307	522.5	136.1	538.6	-	-	-	-13.6	0	0	1	dE3
308	522.3	-317.0	613.5	1497	3	1	-17.5	0	1	0	Sd(onedge)
309	534.7	-479.1	721.4	-	-	-	-13.8	0	0	1	dE2
310	542.1	-435.1	698.5	1373	13	2	-17.8	0	0	0	SB0
312	560.4	176.9	586.0	1890	22	3	-17.8	0	1	0	Scd(onedge)
313	579.4	266.8	635.4	-	-	-	-13.9	0	0	1	dS0(9)
314	566.3	-596.6	826.9	-	-	-	-14.8	1	0	1	dE2,N
315	624.0	607.7	866.4	1071	15	2	-18.7	0	1	0	Sab(rs)II
316	599.7	-344.6	695.0	1546	105	2	-15.0	1	0	1	dE3,N
317	636.1	934.3	1124.7	-	-	-	-13.6	0	0	1	dE1
318	608.4	-306.0	684.0	-	-	-	-15.2	1	0	1	dE2,N
319	648.3	1099.0	1270.0	1445	61	2	-14.9	1	0	1	dE6,N
320	671.0	1115.5	1295.6	-	-	-	-14.0	1	0	1	dE5,N?
321	641.8	-175.9	667.4	-	-	-	-12.5	0	0	1	dE
322	618.8	-1093.1	1262.6	978	15	2	-18.8	0	1	0	Sd
323	642.5	-318.8	720.6	-	-	-	-13.8	0	0	1	dE2/ImV
324	659.4	-356.5	753.4	1493	44	2	-16.0	0	0	1	dS0(8)
325	682.8	148.0	696.9	-	-	-	-13.1	0	0	1	dE3
326	670.4	-452.4	813.4	-	-	-	-12.7	0	0	1	dE1
327	669.9	-724.3	992.8	-	-	-	-13.9	0	0	1	dE3?
328	696.9	-229.4	736.4	-	-	-	-12.9	0	0	1	dE
329	737.8	-175.4	760.6	-	-	-	-13.1	0	0	1	dE
330	759.5	-166.4	779.7	-	-	-	-11.9	0	0	1	dE
331	747.9	-531.9	923.8	-	-	-	-14.2	0	0	1	dE
332	800.8	-172.9	821.6	-	-	-	-15.6	0	0	0	EorS0
334	848.4	70.6	850.2	-	-	-	-12.7	0	0	1	dE(boxy)
335	857.4	-160.3	874.7	1367	24	2	-17.1	0	0	0	E
336	884.0	97.2	887.8	1956	67	2	-13.7	0	0	1	dEpec
337	877.5	-430.6	983.6	-	-	-	-13.5	0	0	1	dE/ImV
338	985.3	691.8	1194.5	1562	16	2	-17.0	0	0	0	S0
339	934.7	-846.3	1272.1	-	-	-	-13.8	1	0	1	dE,N
340	1020.8	-832.1	1329.4	-	-	-	-13.1	0	0	1	dE
470	-773.7	-93.4	780.6	723	79	2	-13.8	0	1	1	S/Im
729	-495.9	135.6	512.9	1676	31	2	-14.8	0	0	1	(d)SO
904	-326.7	310.1	449.2	2254	56	2	-13.9	0	0	1	(d)E
905	-325.3	292.6	436.3	1243	23	2	-13.6	0	1	1	?emission
934	-957.1	705.9	1180.1	1383	85	4	-12.7	0	0	1	E
1005	-231.1	994.2	1019.8	1256	36	2	-17.6	0	0	0	SO
1019	-218.8	738.7	769.7	2013	135	4	-13.0	0	0	1	dS0
1088	-140.7	759.0	771.6	1246	33	4	-12.4	0	1	1	?emission
1108	-120.5	694.5	704.6	1734	21	4	-13.5	0	0	1	(d)SO
1241	-14.5	-20.0	24.7	2012	91	4	-16.6	0	0	1	dE3
1379	104.8	837.0	843.4	745	21	2	-14.0	0	0	1	dE
1554	249.7	35.7	252.1	1642	52	2	-13.6	0	0	1	E
2144	841.7	1114.0	1387.0	1184	25	2	-14.2	0	0	1	(d)E

Notes: The catalogue number (FCC), projected position offsets and radius from the central galaxy NGC 1399 (X, Y, R), absolute magnitude ( $M_B$ ), and morphological type (“morph”) are all taken or calculated from the Fornax Cluster Catalog (Ferguson 1989). The measured radial velocities and uncertainties (cz; err) are from the following references (ref): 1, the NED database; 2, Drinkwater et al. (2001b); 3, Karick (PhD thesis 2003); 4, Drinkwater et al. (2000a). The binary flags for nucleated (nuc), late-type (late) and dwarf galaxies have been derived from the FCC morphology, as described in the text.

along the line of sight:

$$\sigma_{\text{los}}^2(R) = \frac{\int_0^\infty \rho(r)(\sigma_r^2 \sin^2 \theta + \sigma_t^2 \cos^2 \theta) dz}{\int_0^\infty \rho(r) dz} \quad (\text{B1})$$

$$= \sigma_r^2 \left[ 1 - \beta \frac{\int_0^\infty \rho(r) \cos^2 \theta dz}{\int_0^\infty \rho(r) dz} \right] \quad (\text{B2})$$

$$= \sigma_r^2 \left[ 1 - \beta \frac{\int_0^{\pi/2} \rho(r) d\theta}{\int_0^{\pi/2} \frac{\rho(r)}{\cos^2 \theta} d\theta} \right], \quad (\text{B3})$$

where  $z$  measures distance along the line of sight from the midpoint through the cluster and  $r$  is the radius to a point on that line such that  $z = R \tan \theta$  and  $r = R / \cos \theta$ . The value of the integral quotient in equation B3 varies between approximately 0.62 and 0.76 for inner and outer radial bins given in Table 3 (the precise values depend upon the density model for the UCDs but all acceptable fits to the data give similar results).

Table A2 – *continued*

X	Y	R	cz	err	$M_B$
kpc	kpc	kpc	km/s	km/s	mag
21.9	-59.4	63.3	1893	68	-10.2
-60.2	38.8	71.6	2226	87	-10.0
-72.7	-18.6	75.1	1828	77	-10.8
61.2	45.2	76.0	1420	64	-11.1
-6.2	76.7	77.0	1564	73	-11.1
-20.1	-75.3	77.9	1307	63	-10.1
79.3	-8.1	79.7	1920	40	-12.5
-54.0	69.0	87.6	1367	71	-12.4
88.3	0.2	88.3	1448	101	-11.3
-75.8	-53.2	92.7	1496	55	-11.0
-55.7	-83.5	100.5	1175	61	-10.0
81.0	67.8	105.6	1800	93	-10.4
-115.3	-21.1	117.2	1375	46	-10.0
-101.3	-64.3	120.1	1491	39	-11.5
-120.0	-15.1	121.0	1373	92	-10.4
-136.0	43.5	142.7	1817	104	-10.4
131.8	67.0	147.7	1618	73	-10.2
-145.0	29.0	147.8	1350	97	-11.2
-149.9	-55.6	160.0	1462	76	-10.9
-144.1	74.4	162.0	1297	45	-11.1
99.5	131.6	164.8	1355	72	-11.6
-119.4	-125.4	173.4	1340	90	-10.4
77.5	-155.5	173.8	1528	73	-10.6
138.0	118.6	181.8	1433	59	-10.8
152.7	164.9	224.5	1475	57	-10.0
-143.4	177.5	227.9	1658	65	-10.2
220.2	-162.6	274.2	1629	56	-10.3
-256.8	-99.1	275.7	1369	68	-10.3

Notes: The projected position offsets and radius from the central galaxy NGC 1399 (X, Y, R), measured radial velocities and uncertainties (cz; err), and absolute magnitudes ( $M_B$ ), are all taken or calculated from the Fornax Cluster Spectroscopic Survey (Drinkwater et al. 2000a).

This paper has been typeset from a  $\text{\LaTeX}$  file prepared by the author.